Generation, Characterization, and Properties of Iron–Silylene and Iron–Silene Cationic Complexes in the Gas Phase

D. B. Jacobson* and R. Bakhtiar†

Contribution from the Department of Chemistry, North Dakota State University, Fargo, North Dakota 58105-5516

Received April 28, 1993⊛

Abstract: Generation, characterization, and properties of iron–silylene (Fe=SiRR′) and iron–silene (Fe(CH_2=SiRR′)) cations (R, R′ = H, CH_3) are describe in the gas phase by using Fourier transform mass spectrometry (FTMS). Iron–(silylene/silene) cations were formed by reaction of Fe^+ with appropriate silanes. Structures of these ions were probed by using both collision-activated dissociation (CAD) and ion/molecule reactions. CAD failed to yield structural information; however, reaction with isotopically labeled ethene provides *compelling* evidence for formation of iron–silene and iron–silylene species. There is no evidence for the interconversion of iron–silylene and iron–silene species, even upon slow collisional activation or by formation of ethene collision complexes (ca. 40 kcal/mol of excess energy). This indicates that there is a prohibitive barrier for iron mediated interconversion of silene and silylenes. Reactions of iron-silylene and iron-silene species with water and benzene are described. The nature of the bonding is presented and bond dissociation limits are obtained.

Introduction

An obligatory step in many of the transition metal-mediated transformations of organosilanes is oxidative addition across a Si–H bond. Hydrosilation, eq 1, involves the addition of an

$$R_3SiH + R'HC{=}CH_2 \xrightarrow{\text{catalyst}} R'H_2CCH_2SiR_3 \qquad (1)$$

organosilane across a carbon–carbon multiple bond.[1,2] The hydrosilation process requires oxidative addition of Si–H to a transition metal center. The factors important for oxidative addition of a Si–H bond to a transition metal complex have been the focus of recent studies.[3] It has been found that electron withdrawing groups on silane facilitate oxidative addition to $CpMn(CO)_2$.[4,5] In contrast, Zhang, Dobson, and Brown have found that electron donating substituents on the silane facilitate oxidative addition to $Cr(CO)_5$.[6]

The study of the coordination chemistry of transition metal complexes with low-valent silicon ligands has been the focus of intense study in the last 5 years.[7] Transition metal–silylene complexes ($L_nM{=}SiR_2$) are postulated intermediates in a number of transition metal-mediated silane transformations, including Rochow's direct process,[8] catalytic redistribution of silanes,[9] various silylene-transfer reactions,[10] dehydrogenative coupling reactions of silanes,[11,12] and silane polymerization.[13] Although transition metal–carbene,[14] -germylene,[15] –stannylene,[16] and –plumbylene[17] complexes are well-known, the corresponding silylene species have been synthetically elusive. Base stabilized *terminal* transition metal–silylene complexes have recently been generated and characterized.[18–21] Donor stabilized *terminal* silylene complexes were reported by Zybill and Muller[18a] and by

* Author to whom correspondence should be addressed.
† Current address: Chemicals Methods and Separations Group, Battelle Pacific Northwest Laboratories, Richland, WA 99352.
⊛ Abstract published in *Advance ACS Abstracts,* October 1, 1993.

(1) (a) Speier, J. L. *Adv. Organomet. Chem.* **1979**, *17*, 407. (b) Lukevics, E. *Russ. Chem. Rev. (Engl. Transl.)* **1977**, *46*, 264. (c) Ojima, I. In *The Chemistry of Organic Silicon Compounds*; Patia, S., Rappoport, Z., Eds.; Wiley: New York, 1989. (d) Caseri, W.; Pregosin, P. S. *J. Organomet. Chem.* **1988**, *356*, 259. (e) Hostetler, M. J.; Bergman, R. G. *J. Am. Chem. Soc.* **1990**, *112*, 8621.

(2) (a) Harrod, J. F.; Chalk, A. J. In *Organic Synthesis via Metal Carbonyls*; Wender, I., Pino, Pl, Eds.; Wiley: New York, 1977; Vol. 2. (b) Millan, A.; Fernandez, M.; Bentz, P.; Maitlis, P. M. *J. Mol. Catal.* **1984**, *26*, 89. (c) Seitz, F.; Wrighton, M. S. *Angew. Chem., Int. Ed. Engl.* **1988**, *27*, 289. (d) Collman, J. P.; Hegedus, L. S.; Norton, J. R.; Finke, R. G. *Principles and Applications of Organotransition Metal Chemistry*; University Science Books: Mill Valley, CA, 1987. (e) Noll, W. *Chemistry and Technology of Silicones*; Academic Press: New York, 1986.

(3) Schubert, U. *Adv. Organomet. Chem.* **1990**, *30*, 151.

(4) (a) Lichtenberger, D. L.; Rai-Chaudhuri, A. *J. Am. Chem. Soc.* **1989**, *111*, 3583. (b) Lichtenberger, D. L.; Rai-Chaudhuri, A. *J. Am. Chem. Soc.* **1990**, *112*, 249. (c) Lichtenberger, D. L.; Rai-Chaudhuri, A. *Inorg. Chem.* **1990**, *29*, 975.

(5) (a) Schubert, U.; Scholz, G.; Muller, J.; Ackermann, K.; Worle, B.; Stansfield, R. F. D. *J. Organomet. Chem.* **1986**, *300*, 303. (b) Graham, W. A. G. *J. Organomet. Chem.* **1986**, *300*, 81. (c) Carre, F.; Colomer, E.; Corriu, R. G. P.; Viouz, A. *Organometallics* **1984**, *3*, 1272.

(6) Zhang, S.; Dobson, G. R.; Brown, T. L. *J. Am. Chem. Soc.* **1991**, *113*, 6908.

(7) (a) Tilley, T. D. In *The Chemistry of Organic Silicon Compounds*; Patai, S., Rappoport, Z., Eds.; John Wiley and Sons: New York, 1989, Chapter 24. (b) Tilley, T. D. In *The Silicon Heteroatom Bond*; Patai, S., Rappoport, Z., Eds.; John Wiley: New York, 1991; p 309. (c) Zybill, C. *Top. Curr. Chem.* **1992**, *160*, 1. (d) Zybill, C. *Nachr. Chem. Tech. Lab.* **1989**, *37*, 248.

(8) Buechner, W. J. *J. Organomet. Chem. Lib.* **1980**, *9*, 409.

(9) (a) Curtis, M. D.; Epstein, P. S. *Adv. Organomet. Chem.* **1981**, *19*, 213. (b) Yamamoto, K.; Okinshima, H.; Kumada, M. *J. Organomet. Chem.* **1971**, *27*, C31. (c) Ojima, I.; Inaba, S.-I.; Kogure, T.; Nagai, Y. *J. Organomet. Chem.* **1973**, *55*, C7. (d) Kumada, M. *J. Organomet. Chem.* **1975**, *100*, 127.

(10) (a) Okinoshima, H.; Yamamoto, K.; Kumada, M. *J. Am. Chem. Soc.* **1972**, *94*, 9263. (b) Sakurai, H.; Kamiyama, Y.; Nakadaira, Y. *J. Am. Chem. Soc.* **1977**, *99*, 3879. (c) Pannell, K. H.; Cervantes, J.; Hernandez, C.; Cassias, J.; Vincenti, S. *Organometallics* **1986**, *5*, 1056 and references cited therein. (d) Tobita, H.; Ueno, K.; Ogino, H. *Chem. Lett.* **1986**, 1777. (e) Tobita, H.; Ueno, K.; Ogino, H. *Bull. Chem. Soc. Jpn.* **1988**, *61*, 2797. (f) Thum. G.; Malisch, W. *J. Organomet. Chem.* **1984**, *264*, C5.

(11) Brown-Wensley, K. *Organometallics* **1987**, *6*, 1590.

(12) (a) Harrod, J. F. *Polyhedron* **1991**, *10*, 1239. (b) Chang, L. S.; Corey, J. Y. *Organometallics* **1989**, *8*, 1885. (c) Corey, J. Y.; Chang, L. S.; Corey, E. R. *Organometallics* **1987**, *6*, 1595.

(13) (a) Anderson, A. B.; Shiller, P.; Zarate, E. A.; Tessler-Youngs, C. A.; Youngs, W. J. *Organometallics*, **1989**, *8*, 2320 and references cited therein. (b) Woo, H.-G.; Walzer, J. F.; Tilley, T. D. *J. Am. Chem. Soc.* **1992**, *114*, 7047 and references cited therein.

(14) (a) Fischer, E. O. *Adv. Organomet. Chem.* **1976**, *14*, 1. (b) Casey, C. P. In *Reactive Intermediates*; Jones, M., Jr.; Moss, R. A., Eds.; Wiley: New York, 1981; Vol. II, p 135.

(15) (a) Lappert, M. F. *Rev. Silicon, Germanium, Tin, Lead Compd* **1986**, *9*, 129. (b) Petz, W. *Chem. Rev.* **1986**, *86*, 1019 and references cited therein.

(16) (a) Hichcock, P. B.; Lappert, M. F.; Misra, M. C. *J. Chem. Soc., Chem. Commun.* **1985**, 863. (b) Lappert, M. F.; Power, P. P. *J. Chem. Soc., Dalton Trans.* **1985**, 51 and references cited therein.

(17) (a) Hermann, W. A.; Kneuper, H.-J.; Herdtweck, E. *Angew. Chem., Int. Ed. Engl.* **1985**, *24*, 1062. (b) Cotton, J. D.; Davidson, P. J.; Lappert, M. F. *J. Chem. Soc., Dalton Trans.* **1976**, 2275.

(18) (a) Zybill, C.; Muller, G. *Angew. Chem., Int. Ed. Engl.* **1987**, *26*, 669. (b) Zybill, C.; Muller, G. *Organometallics* **1988**, *7*, 1368. (c) Zybill, C.; Wilkinson, D. L.; Leis, C.; Muller, G. *Angew. Chem., Int. Ed. Engl.* **1988**, *27*, 583. (d) Zybill, C.; Wilkinson, D. L.; Leis, C.; Muller, G. *Angew. Chem., Int. Ed. Engl.* **1989**, *28*, 203. (e) Zybill, C. *Top. Curr. Chem.* **1991**, *160*, 1. (f) Handwerker, H.; Leis, C.; Siegfried, G.; Zybill, C. *Inorg. Chim. Acta* **1992**, *198–200*, 763. (g) Probst, R.; Leis, C.; Gampers, S.; Herdweck, W. E.; Zybill, C.; Auner, N. *Angew. Chem., Int. Ed. Engl.* **1991**, *30*, 1132.

0002-7863/93/1515-10830$04.00/0

Tilley and co-workers[19a] in 1987. Base free silylene complexes have only recently been synthesized and characterized.[22] Due to the electrophilic nature of the silylene fragment, most of the stable transition metal–silylene complexes consist of electron rich metal complexes in low oxidation states.

The related transition metal–silene complexes ($L_nM(R_2Si{=}CH_2)$) have been proposed as intermediates in metal-mediated rearrangement of organosilicon ligands,[23] including β-hydrogen transfer from a bound silyl group.[24,25] The first example of a metal–silene complex was reported by Wrighton[25] and involved β-hydrogen migration from the unsaturated complex, $(C_5R_5)(CO)_2W{-}SiMe_3$, to yield $(C_5R_5)(CO)_2W(H){-}(CH_2{=}SiMe_2)$ in a hydrocarbon matrix at 77 K. Depending upon the extent of back donation, η^2-silene complexes can be characterized either as silametallacyclopropane (**1**) or π-silene complexes (**2**). Recently, Randolph and Wrighton reported the involvement of the

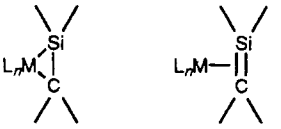

1 **2**

silene, $(C_5R_5)(CO)Fe(CH_2{=}SiMe_2)H$, as an intermediate in the photochemical rearrangement of $(C_5R_5)(CO)_2FeCH_2SiMe_2H$ to $(C_5R_5)(CO)_2FeSiMe_3$ at low temperature.[25b] Stable transition metal–silene complexes have recently been synthesized and characterized.[26,27]

The difficulty in synthesizing stable intermediates, particularly metal–silylene complexes, has prevented detailed studies concerning their involvement in organosilane transformations. The ability to study model systems will be invaluable in understanding these processes and in gaining insight into designing systems to increase process selectivity and efficiency. Gas phase ion techniques have proven to be well suited for generating and studying the chemical and physical properties of reactive transition metal species.[28] For example, the reaction of atomic transition metal ions with hydrocarbons has been studied in detail.[29] In this report, we describe the generation, characterization, and properties of iron–silylene and iron–silene cationic complexes in the gas phase. The reaction of atomic metal ions (Ti^+, V^+, Cr^+, Fe^+, Co^+, and Ni^+) with simple methylsilanes in the gas phase has been reported.[30] Recently, we reported that isomeric iron–silylene and iron–silene cationic complexes can be structurally characterized by specific ion/molecule reactions in the gas phase.[31]

Table I. Lower Electronic States of Fe^+ (below 2.5 eV)

state	config	energy,[a] eV
^6D	$4s3d^6$	0.052
^4F	$3d^7$	0.300
^4D	$4s3d^6$	1.032
^4P	$3d^7$	1.688
^2G	$3d^7$	1.993
^2P	$3d^7$	2.298

[a] Statistical average over all J states. Energies taken from ref 76.

Experimental Section

All experiments were performed by using a modified Nicolet FTMS-1000 Fourier transform mass spectrometer[32,33] equipped with a 5.08-cm cubic trapping cell and a 3.0 T superconducting magnet.[34] A Bayard/Alpert type ionization gauge was used to monitor pressure and was calibrated by using reactions with well-known rate constants. The pressure of reagent neutrals was subsequently corrected by using ionization cross sections.[35] Absolute pressure uncertainties are believed to be <50% for organosilanes and <30% for other organic species.[36] The uncertainty in pressure is the largest contributor to the uncertainty in measured rate constants. Consequently, rate constants are assigned an absolute error of ±50% for reactions with organosilanes and ±30% for reaction with other organic reagents. Ethene-d_4 and ethene-$^{13}C_2$ were obtained from MSD Isotopes with >98% isotopic purity. Organosilanes were either obtained commercially or prepared by reduction of the corresponding chloride with $LiAlH_4$ or $LiAlD_4$[37] and purified by vacuum distillation. 1,1-Dimethylsilacyclobutane-*1,1,1,1,1,1-d*$_6$ was prepared by reaction of 1,1-dichlorosilacyclobutane with CD_3MgI[38] with product purity confirmed by NMR and GC-MS. All liquid reagents were subjected to multiple freeze–pump–thaw cycles to remove noncondensable gases.

Fe^+ was generated by laser desorption/ionization from a high purity iron foil attached to the rear trapping plate of the cell.[39] The kinetics for reaction of Fe^+ with organosilanes was obtained by using a static pressure of the organosilane. Laser desorption/ionization may generate excited Fe^+. Reaction kinetics and product branching ratios were obtained by first trapping the laser generated Fe^+ for 1 s in the presence of silane. Fe^+ was then isolated by swept ejection pulses[32] and then allowed to react with silane. This approach should minimize the role of excited Fe^+ (Table I) on the observed chemistry.

The structure of ions produced by reaction of Fe^+ with various silanes was probed by reaction with selected reagents. For these structural studies the precursor silane was admitted into the vacuum chamber *via* a pulsed solenoid inlet valve[40] in order to minimize complicating side reactions with background silane. The pulsed valve was triggered off the quench

(19) (a) Straus, D. A.; Tilley, T. D.; Rheingold, A. L.; Geib., S. *J. Am. Chem. Soc.* **1987**, *109*, 5872. (b) Straus, D. A.; Zhang, C.; Quimbita, N.; Grumbine, S. D.; Heyn, R. H.; Tilley, T. D.; Rheingold, A. L.; Geib. S. J. *J. Am. Chem. Soc.* **1990**, *112*, 2673.

(20) (a) Ueno, K.; Tobita, H.; Shimoi, M.; Ogino, H. *J. Am. Chem. Soc.* **1988**, *110*, 4092. (b) Tobita, H,; Ueno, K.; Shimoi, M.; Ogino, H. *J. Am. Chem. Soc.* **1990**, *112*, 3415.

(21) Woo, L. K.; Smith, D. A.; Young, V. G., Jr. *Organometallics* **1991**, *10*, 3977.

(22) (a) Jutzi, P.; Mohrke, A. *Angew. Chem., Int. Ed. Engl.* **1990**, *29*, 893. (b) Straus, D. A.; Grumbine, S. D.; Tilley, T. D. *J. Am. Chem. Soc.* **1990**, *112*, 7801. (c) Lee, K. E.; Arif, A. M.; Gladysz, J. A. *Chem. Ber.* **1991**, *124*, 309.

(23) (a) Pannell, K. H. *J. Organomet. Chem.* **1970**, *21*, 17. (b) Pannell, K. H.; Rice, J. R. *J. Organomet. Chem.* **1974**, *78*, C35. (c) Windus, C.; Sujishi, S.; Giering, W. P. *J. Am. Chem. Soc.* **1974**, *96*, 1951. (d) Bulkowski, J. E.; Miro, N. D.; Sepelak, D.; Van Dyke, C. H. *J. Organomet. Chem.* **1975**, *101*, 267. (e) Ramao, K.; Yoshida, J.; Okazaki, S.; Kumada, M. *Isr. J. Chem.* **1976/1977**, *15*, 265. (f) Ishikawa, M.; Ohshita, J.; Ito, Y. *Organometallics* **1986**, *5*, 1518.

(24) Berry, D. H.; Procopio, L. J. *J. Am. Chem. Soc.* **1989**, *111*, 4099.

(25) (a) Lewis, C.; Wrighton, M. S. *J. Am. Chem. Soc.* **1983**, *105*, 7768. (b) Randolph, C. L.; Wrighton, M. S. *Organometallics* **1987**, *6*, 365.

(26) (a) Campion, B. K.; Heyn, R. H.; Tilley, T. D. *J. Am. Chem. Soc.* **1988**, *110*, 7558. (b) Campion, B. K.; Heyn, R. H.; Tilley, T. D. *J. Am. Chem. Soc.* **1990**, *112*, 4079. (c) Campion, B. K.; Heyn, R. H.; Tilley, T. D. *J. Chem. Soc., Chem. Commun.* **1992**, 1201.

(27) (a) Procopio, L. J.; Berry, D. H. *J. Am. Chem. Soc.* **1991**, *113*, 4039. (b) Koloski, T. S.; Carroll, P. J.; Berry, D. H. *J. Am. Chem. Soc.* **1990**, *112*, 6405. (c) Ando, W.; Yamamoto, T.; Saso, H.; Kabe, Y. *J. Am. Chem. Soc.* **1991**, *113*, 2791.

(28) *Gas Phase Inorganic Chemistry*; Russell, D. H., Ed.; Plenum Press: New York, 1989.

(29) (a) Eller, K.; Schwarz, H. *Chem. Rev.* **1991**, *91*, 1121. (b) Armentrout, P. B. *Annu. Rev. Phys. Chem.* **1990**, *41*, 313. (c) Armentrout, P. B.; Beauchamp, J. L. *Acc. Chem. Res.* **1989**, *22*, 315.

(30) Kang, H.; Jacobson, D. B.; Shin, S. K.; Beauchamp, J. L.; Bowers, M. T. *J. Am. Chem. Soc.* **1986**, *108*, 5668.

(31) Bakhtiar, R.; Holznagel, C. M.; Jacobson, D. B. *J. Am. Chem. Soc.* **1993**, *115*, 345.

(32) For reviews on FTMS, see: (a) Gross, M. L.; Rempel, D. L. *Science (Washington,D.C.)* **1984**, *226*, 26. (b) Wanczek, K.-P. *Int. J. Mass Spectrom. Ion Processes* **1989**, *95*, 1. (c) Marshall, A. G. *Acc. Chem. Res.* **1985**, *18*, 316. (d) Comisarow, M. B. *Anal. Chim. Acta* **1985**, *178*, 1. (e) Nibbering, N. M. M. *Acc. Chem. Res.* **1990**, *23*, 279. (f) Marshall, A. G.; Grosshans, P. B. *Anal. Chem.* **1991**, *63*, 215A.

(33) *Fourier Transform Mass Spectrometry*; Buchanan, M. V., Ed.; American Chemical Society: Washington, DC, 1987.

(34) Jacobson, D. B. *J. Am. Chem. Soc.* **1989**, *111*, 1626.

(35) Bartmess, J. E.; Geordiadis, R. M. *Vacuum* **1983**, *33*, 149.

(36) Ionization efficiencies for silanes were determined from estimated polarizabilites (Otvos, J. W.; Stevenson, D. P. *J. Am. Chem. Soc.* **1956**, *78*, 546) and subsequent corrections (ref 35). As a consequence, we assign a significant (±50%) error in the absolute pressure of silanes.

(37) Gaspar, P. P.; Levy, C. A.; Adair, G. M. *Inorg. Chem.* **1970**, *9*, 1272.

(38) Sommer, L. H. *J. Am. Chem. Soc.* **1946**, *68*, 485.

(39) (a) Burnier, R. C.; Byrd, G. D.; Freiser, B. S. *J. Am. Chem. Soc.* **1981**, *103*, 4360. (b) Byrd, G. D.; Burnier, R. C.; Freiser, B. S. *J. Am. Chem. Soc.* **1982**, *104*, 3565.

(40) A detailed description of pulsed valve introduction of reagent gases in conjunction with FTMS can be found in the following: Carlin, T. J.; Freiser, B. S. *Anal. Chem.* **1983**, *55*, 571.

Table II. Percentages of Neutrals Lost and Adduct Formation in the Primary Reaction of Fe^+ with Organosilanes

	Neutrals Lost											
Organosilane	H_2	HD	D_2	CH_4	CH_3D	SiH_4	C_2H_4	C_3H_6	$(CH_3)SiH_3$	$(CH_3)_3SiH$	$(CH_3)_4Si$	adduct
$(CH_3)SiH_3$												100
$(CH_3)_2SiH_2$	90											10
$(CH_3)_2SiD_2$			65									35
$(CH_3)_3SiH^a$	35			55								10
$(CH_3)_3SiD^b$	2	32			50							16
$(CH_3)_4Si$												100
$CH_2CHSi(CH_3)H_2$	10						83		6			1
Si_2H_6						99						1
$Si_2(CH_3)_6$	5			5						15	74	1
silacyclobutane							96					4
1-silacyclobutane-*1,1-d*$_2$							98					2
1-methylsilacyclobutane							100					
1,1-dimethylsilacyclobutane							97	3				

[a] A trace (<1%) of $(CH_3)_3Si^+$ (corresponding to FeH loss) was observed. [b] A trace (<1%) of $(CH_3)_3Si^+$ (corresponding to FeD loss) was observed.

pulse with the valve duration varied (typically between 2 and 3 ms) to control the amount of pulsed reagents. The ballast pressure in the pulsed valve assembly was <1 Torr. A variable delay after triggering the pulsed valve (ca. 1 s) was used to allow the pulsed organosilane reagent to be removed from the vacuum chamber followed by isolation of the desired product ions. The isolated ions were then reacted with specific neutral reagents or were subjected to fragmentation by collision-activated dissociation (CAD).[41] A static pressure of 1×10^{-5} Torr of Ar was used throughout these experiments and served as the facilitator of ion thermalization prior to reaction and as the target for CAD.[41]

Details of CAD in conjunction with FTMS have been described elsewhere.[42] CAD breakdown curves were obtained by varying the kinetic energy of the ions (typically between 1 and 50 eV) by adjusting the duration of the electric field pulse (typically between 100 and 600 μs). The maximum kinetic energy acquired by an irradiated ion (in excess of thermal energy) was calculated by using the relationship

$$E_{tr}(\max) = (E_{Rf})^2 e^2 t^2 / 8m \qquad (2)$$

where E_{Rf} is the electric field amplitude, e is the electric charge, t is the duration of the electric field pulse, and m is the mass of the ion.[43,44] CAD fragment ion intensities are plotted as a fraction of the initial parent ion intensity (no excitation) versus kinetic energy. This allows both the energy dependency for fragmentation and the fragmentation efficiency to be compared directly for related systems. CAD breakdown curves are reproducible with <3% absolute variation in ion abundances for replicate curves. The spread in ion kinetic energy is dependent on the total average kinetic energy and is 65% at 1 eV, 19% at 10 eV, 11% at 30 eV, and 6% at 100 eV.[45]

In addition to conventional *resonant* FTMS-CAD, CAD by using sustained "off-resonance" irradiation (SORI) for ion activation was investigated where the translational energy of an irradiated ion is given by

$$E_{tr} = \{(E_{Rf})^2 e^2 / [2m(\omega - \omega_c)^2]\} \sin^2[(\omega - \omega_c)t/2] \qquad (3)$$

where ω(rad/s) is the excitation frequency and ω_c is the natural cyclotron frequency of the ion[43] (other variables same as listed above). A consequence of "off-resonance" irradiation is that an ion undergoes acceleration/deceleration cycles throughout the duration of the electric field pulse. Hence, ions can be irradiated for an extended period while a low *maximum* translational energy is maintained. When a long duration (500 ms) "off-resonance" electric field pulse and an appropriate $\Delta\omega$ ($\Delta\omega = \omega - \omega_c$) are used, an ion can be slowly collisionally activated by sequential, inelastic collisions prior to fragmentation.[46,47] This method of ion activation (SORI-CAD) is analogous to infrared multiphoton dissociation (IRMPD) for probing the lowest energy pathway for ion dissociation.[48] The lowest energy pathway for dissociation of ions was studied by using SORI-CAD, employing a 500-ms electric field pulse and appropriate $\Delta\omega$.

Table III. Summary of Kinetic Data for Reaction of Fe^+ with Organosilanes

organosilane	k^a	eff[b]
SiH_4	no reaction	
$(CH_3)SiH_3$	0.014 (0.007)	0.0014
$(CH_3)_2SiH_2$	2.0 (1.0)	0.18
$(CH_3)_2SiD_2$	1.0 (0.5)	0.09
$(CH_3)_3SiH$	6.1 (3.0)	0.61
$(CH_3)_3SiD$	6.9 (3.4)	0.68
$(CH_3)_4Si$	2.5 (1.2)	0.27
$CH_2CHSi(CH_3)H_2$	12 (6)	1.1
Si_2H_6	13 (6)	1.4
$Si_2(CH_3)_6$	18 (9)	1.4
silacyclobutane	10 (5)	0.92
silacyclobutane-*1,1-d*$_2$	8.9 (4)	0.83
1-methylsilacyclobutane	16 (8)	1.6
1,1-dimethylsilacyclobutane	16 (8)	1.4

[a] Observed bimolecular rate coefficient for disapparance of reactant ion in the units of 10^{-10} cm^3 molecule^{-1} s^{-1} with uncertainty of ±50% (in parentheses). [b] Overall reaction efficiency = k_{obs}/k_{coll}. Collision rates calculated by using the average dipole orientation approximation taken from ref 77.

Results and Discussion

Reaction of Fe^+ (^6D) with Silanes. The distribution of neutrals lost for reaction of Fe^+ with silanes is summarized in Table II. All reactions yield pseudo-first order kinetics with rate constants and reaction efficiencies listed in Table III. Reaction efficiencies range from a low of 0.0014 to a high of 1.6. The results for reaction with $(CH_3)_xSiH_{4-x}$ (x = 0–4) and $(CH_3)_6Si_2$ agree with a previous report using an ion beam instrument.[30] In many cases, formation of stable adducts (no neutral loss occurs) is observed (Table II). This observation suggests that the ion/molecule collision complexes are long lived and, as a consequence, are stabilized by either infrared radiative emission[49,50] or collisional stabilization with argon (ca. 6 ms/collision). Collisional stabi-

(41) (a) Cooks, R. G. *Collision Spectroscopy*; Plenum Press: New York, 1978. (b) Busch, K. L.; Glish, R. L.; McLuckey, S. A. *Mass Spectrometry/Mass Spectrometry*; VCH:New York, 1988.

(42) For discussions of CAD involving FTMS, see: (a) McIver, R. T., Jr.; Bowers, W. D. In *Tandem Mass Spectrometry*; McLafferty, F. W., Ed.; Willey: New York, 1983; p 287. (b) Cody, R. B.; Burnier, R. C.; Freiser, B. S. *Anal. Chem.* **1982**, *54*, 96. (c) Burnier, R. C.; Cody, R. B.; Freiser, B. S. *J. Am. Chem. Soc.* **1982**, *104*, 7436.

(43) Beauchamp, J. L. *Annu. Rev. Phys. Chem.* **1971**, *22*, 527.

(44) It has been suggested that the kinetic energy obtained by an irradiated ion is much less than that calculated from eq 2: Grosshans, P. B.; Shields, P.; Marshall, A. G. *J. Am. Chem. Soc.* **1990**, *112*, 1275.

(45) Comisarow, M. B. *J. Chem. Phys.* **1971**, *55*, 187.

(46) Gauthier, J. W.; Trautman, T. R.; Jacobson, D. B. *Anal. Chim. Acta* **1991**, *246*, 211.

(47) A CAD method similar to SORI-CAD for FTMS has been described and employs irradiation of the ion at its natural cyclotron frequency with a series of 180° phase shifts resulting in acceleration/deceleration of the irradiated ions: Boering, K. A.; Rolfe, J.; Brauman, J. I. *Int. J. Mass Spectrom. Ion Processes* **1992**, *117*, 357.

(48) Thorne, L. R.; Beauchamp, J. L. In *Gas Phase Ion Chemistry*; Bowers, M. T., Ed.; Academic Press: New York, 1984; Vol. 3, p 41.

(49) Woodin, R. L.; Beauchamp, J. L. *Chem. Phys.* **1979**, *41*, 1.

(50) Dunbar, R. C. *Int. J. Mass Spectrom. Ion Phys.* **1983**, *54*, 109.

Scheme I

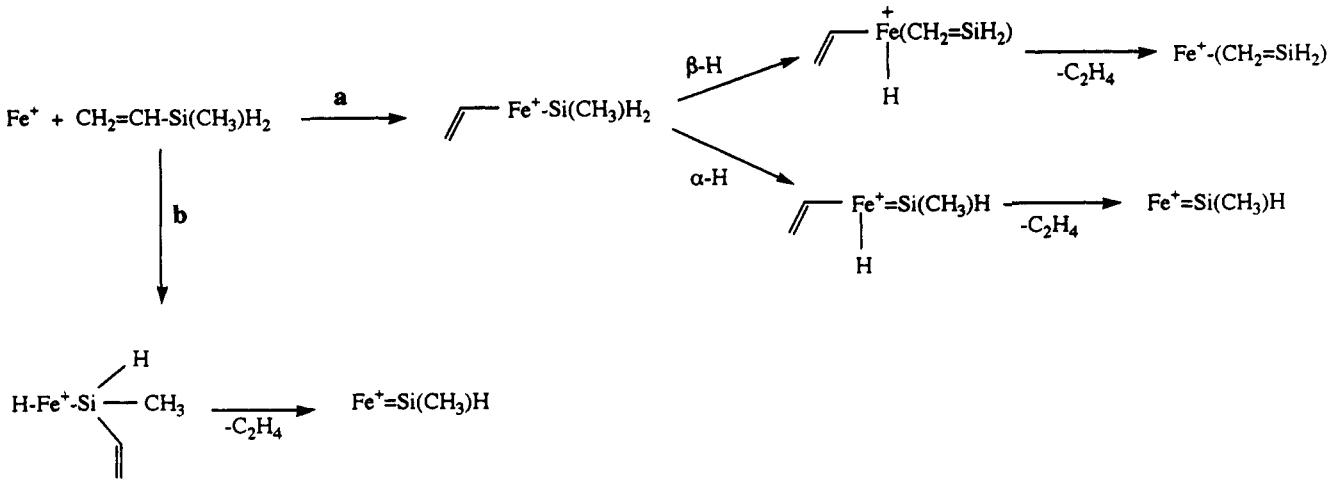

Scheme II

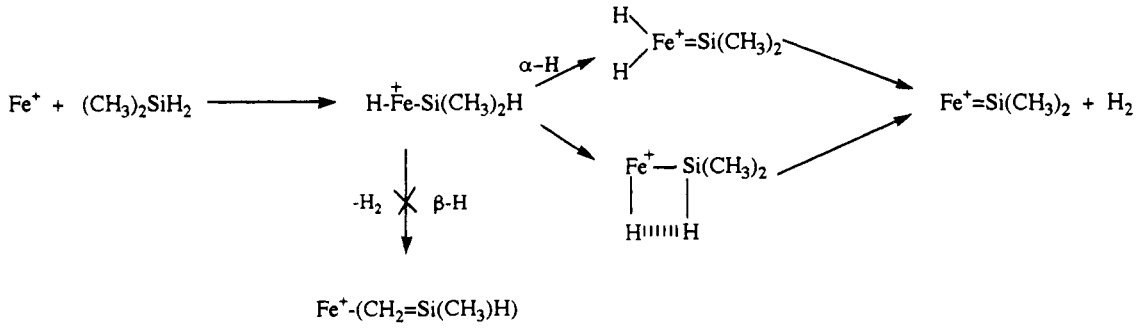

lization with argon seems unlikely due to the long average time between collisions. Adduct formation is the exclusive process observed with $(CH_3)SiH_3$ and $(CH_3)_4Si$. The efficiency for adduct formation with $(CH_3)_4Si$ is unusually high (eff. = 0.27). There are dramatic differences in both the reaction efficiency and the amount of adduct formation for $(CH_3)_2SiH_2$ and $(CH_3)_2SiD_2$ (Tables II and III). These differences may be due to kinetic isotope effects, where it is more difficult for insertion into a Si–D bond than into a Si–H bond for dimethylsilane (k_H/k_D = 2.2). This would then yield a greater probability for adduct formation with $(CH_3)_2SiD_2$ and an overall lower reaction efficiency. Alternatively, the greater degree of adduct formation with $(CH_3)_2SiD_2$ may be due to more efficient radiative emission for the collision complex. In contrast, there are only slight differences for reaction of Fe^+ with $(CH_3)_3SiH$ and $(CH_3)_3SiD$ (Tables II and III).

The major reaction channel with $(CH_2CH)(CH_3)SiH_2$ is C_2H_4 elimination, reaction 4. A proposed mechanism for reaction 4 is

$$Fe^+ + (CH_2CH)(CH_3)SiH_2 \rightarrow \underset{\textbf{3a}}{FeSiCH_4^+} + C_2H_4 \quad (4)$$

presented in Scheme I and involves initial insertion into either a vinylic C–Si bond (path a) or a Si–H bond (path b). Ethene elimination (path a) may proceed by either α-hydrogen or β-hydrogen migration. The 1,1-elimination process predicts formation of an iron–silylene complex, whereas the 1,2-elimination process predicts iron–silene formation. Ethene elimination by initial Si–H insertion should yield an iron–silylene complex (path b).

Dehydrogenation is the only elimination product observed for $(CH_3)_2SiH_2$, reaction 5. Specific elimination of D_2 with $(CH_3)_2SiD_2$ suggests formation of an iron–silylene complex in reaction 5.[30] A proposed mechanism for dehydrogenation of $(CH_3)_2SiH_2$

$$Fe^+ + (CH_3)_2SiH_2 \rightarrow \underset{\textbf{4a}}{FeSiC_2H_6^+} + H_2 \quad (5)$$

is illustrated in Scheme II and involves initial insertion into a Si–H bond (Si–D) followed by dehydrogenation (a 1,1-elimination process). The absence of HD loss with $(CH_3)_2SiD_2$ indicates that β-hydrogen migration is not operative. Both dehydrogenation and demethanation are significant processes for reaction with $(CH_3)_3SiH$, reaction 6. These processes may proceed by initial

$$Fe^+ + (CH_3)_3SiH \rightarrow \begin{cases} FeSiC_3H_8^+ + H_2 & (6a) \\ FeSiC_2H_6^+ + CH_4 & (6b) \end{cases}$$

insertion into the Si–H bond followed by either demethanation (a 1,1-elimination process) or dehydrogenation (a 1,2-elimination process), Scheme III. Scheme III predicts formation of iron–silene and iron–silylene complexes by reactions 6a and 6b, respectively. Reaction with $(CH_3)_3SiD$ yields specific elimination of methane as CH_3D and supports formation of an iron–silylene complex in reaction 6b. Predominant dehydrogenation as HD loss from $(CH_3)_3SiD$ suggests formation of an iron–silene complex in reaction 6a. The small amount of H_2 loss with $(CH_3)_3SiD$ can be accounted for by invoking reversible β-hydrogen migration/silene insertion, Scheme III. The absence of neutral losses for reaction with $(CH_3)_4Si$ combined with exclusive 1,1-dehydrogenation of $(CH_3)_2SiH_2$ suggest that insertion into the Si–CH_3 bond of methylsilanes is unfavorable and supports the proposed mechanism in Scheme III. The higher reaction efficiency for $(CH_2CH)(CH_3)SiH_2$ than for either $(CH_3)_2SiH_2$ or $(CH_3)_3SiH$ suggests that insertion into the vinylic Si–C bond is a more favorable process than insertion into a Si–H bond.

Scheme III

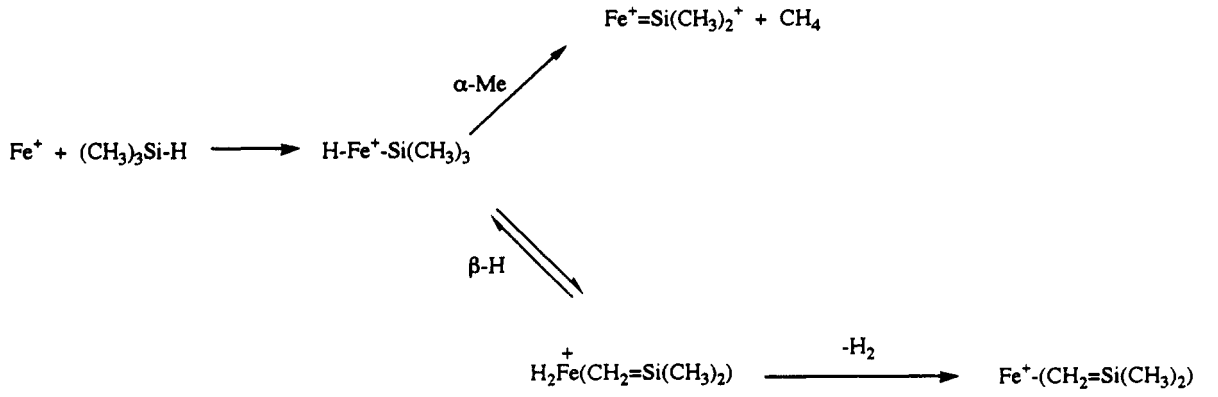

Scheme IV

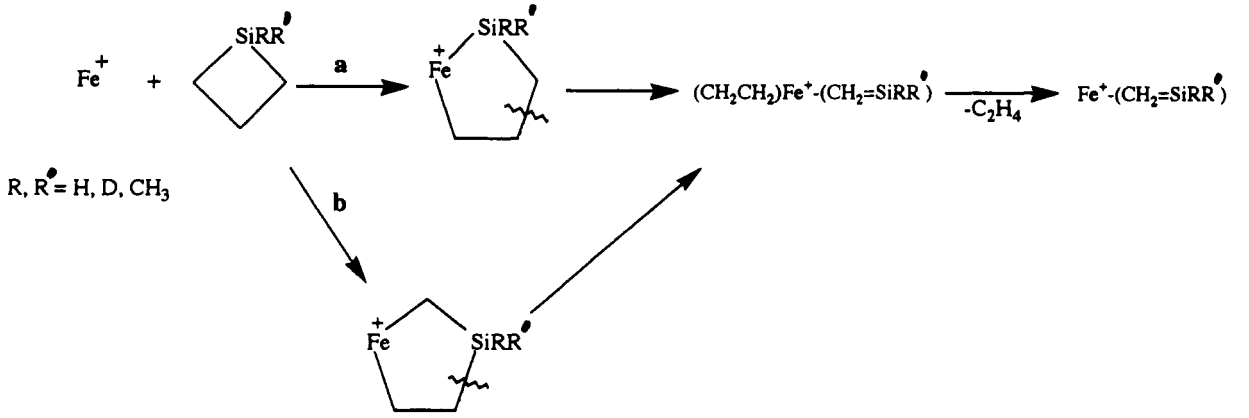

The predominant reaction with silacyclobutanes is elimination of C_2H_4, reactions 7–9. A mechanism for ethene extrusion from

$$Fe^+ + \square SiH_2 \longrightarrow \underset{\mathbf{3b}}{FeSiCH_4^+} + C_2H_4 \qquad (7)$$

$$Fe^+ + \square Si(CH_3)H \longrightarrow \underset{\mathbf{4b}}{FeSiC_2H_6^+} + C_2H_4 \qquad (8)$$

$$Fe^+ + \square Si(CH_3)_2 \longrightarrow \underset{\mathbf{5}}{FeSiC_3H_8^+} + C_2H_4 \qquad (9)$$

silacyclobutanes is presented in Scheme IV and involves initial insertion into a strain weakened Si–C bond[51,52] (path a) to yield a silametallacyclopentane[53] followed by ethene elimination.[54] Alternatively, ethene extrusion may proceed by initial insertion into the strain weakened C1–C2 bond of the ring (path b) with subsequent ethene elimination, Scheme IV. Both processes, however, would generate identical iron–silene complexes, and these pathways cannot be distinguished by isotopic labeling. Exclusive loss of C_2H_4 with 1-silacyclobutane-*1,1-d*$_2$, reaction 10, is consistent with formation of an iron–silene complex in

$$Fe^+ + \square SiD_2 \longrightarrow \underset{\mathbf{3c}}{FeSiCH_2D_2^+} + C_2H_4 \qquad (10)$$

reaction 7. The absence of both dehydrogenation and demethanation channels for reaction with either silacyclobutane or 1-methylsilacyclobutane indicates that insertion into the strain weakened Si–C or C–C bonds is more favorable than insertion into Si–H bonds.

The major reaction channels for $(CH_3)_6Si_2$ and Si_2H_6 are listed in reactions 11 and 12. These reactions may proceed by initial

$$Fe^+ + (CH_3)_6Si_2 \longrightarrow \begin{cases} FeSiC_2H_6^+ + (CH_3)_4Si & (11a) \\ FeSiC_3H_8^+ + (CH_3)_3SiH & (11b) \end{cases}$$

$$Fe^+ + Si_2H_6 \longrightarrow FeSiH_2^+ + SiH_4 \qquad (12)$$

insertion into the Si–Si bond followed by simple group migration, Schemes V and VI. Schemes V and VI predict formation of iron–silylene and iron–silene complexes.

Structural Studies. Schemes I–VI predict formation of iron–silene and iron–silylene complexes. The structures of $FeSiH_2^+$, $FeSiCH_4^+$, $FeSiC_2H_6^+$, and $FeSiC_3H_8^+$ ions were probed by both collision activated dissociation (CAD)[41,42] and specific ion/molecule reactions.

$FeSiH_2^+$. $FeSiH_2^+$, produced in reaction 12, may be formulated as either a silylene complex (**6a**) or the hydrido species (**6b** and **6c**). CAD yields predominant dehydrogenation with some Fe^+

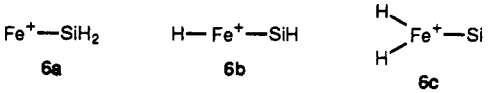

formation at high kinetic energy, reaction 13 (Figure 1). SORI-CAD yields exclusive dehydrogenation, reaction 13a, indicating

$$FeSiH_2^+ \xrightarrow{CAD} \begin{cases} FeSi^+ + H_2 & (13a) \\ Fe^+ + (SiH_2) & (13b) \end{cases}$$

(51) Silacyclobutanes and cyclobutanes have similar ring strain energies (ca. 26 kcal/mol): Sokolova, E. V.; Danilova, T. F.; Shvets, G. N.; Guselnikov, L. E.; Volkova, V. V.; Klyuchnikov, V. A.; Voronkev, M. G. *Metalloorg. Khim.* **1991**, *4*, 97.

(52) (a) Curtis, M. D.; Epstein, P. S. *Adv. Organomet. Chem.* **1981**, *19*, 213. (b) Seyferth, D.; Shannon, M. L.; Vick, S. C.; Lim, T. F. O. *Organometallics* **1985**, *4*, 57.

(53) (a) Cundy, C. S.; Lappert, M. F.; Dubac, J.; Mazerolles, P. *J. Chem. Soc., Dalton Trans.* **1976**, 910. (b) Schubert, U.; Reongste, A. *J. Organomet. Chem.* **1979**, *170*, C37.

(54) Gentle, R. M.; Muetterties, E. L. *J. Am. Chem. Soc.* **1983**, *105*, 304.

Scheme V

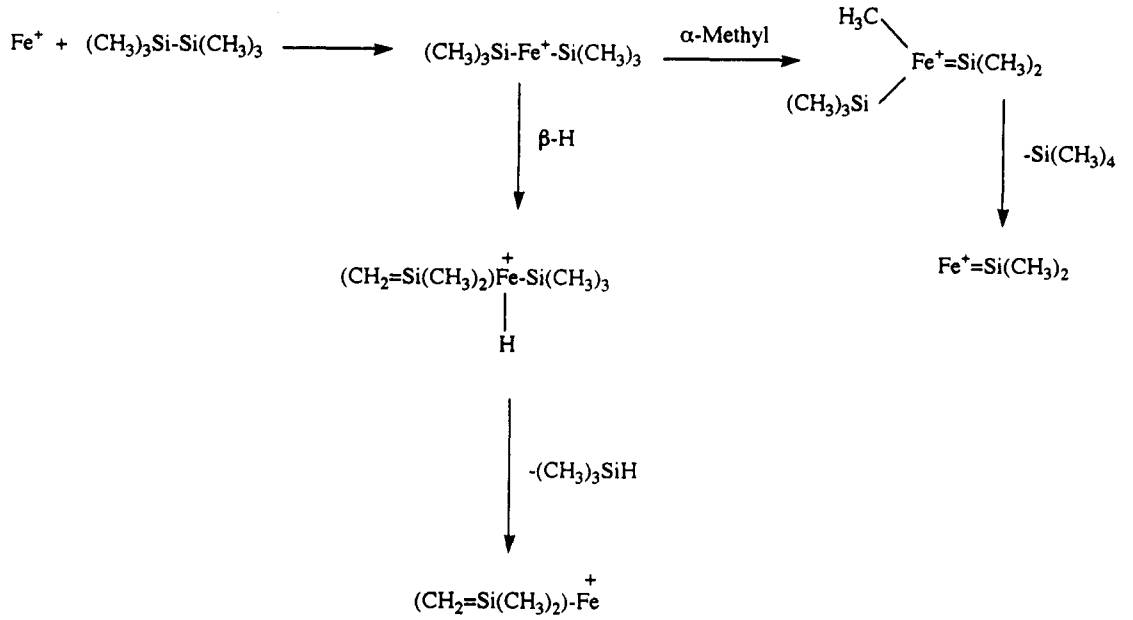

Scheme VI

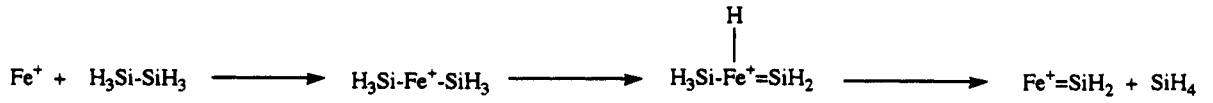

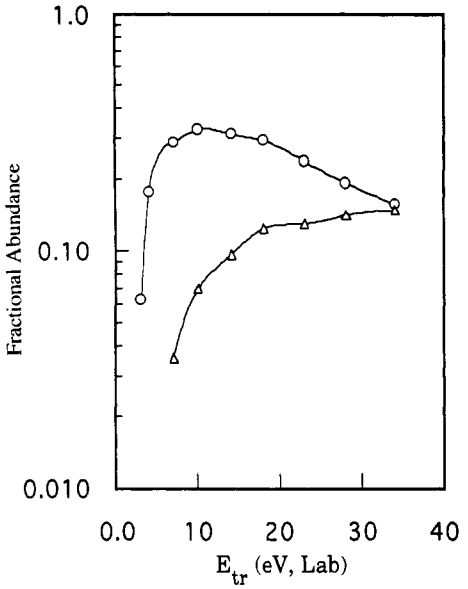

Figure 1. Plot of the variation of fragment ion abundances as a function of kinetic energy (laboratory frame) for CAD of $FeSiH_2^+$: $FeSi^+$ (○), Fe^+ (△).

that it is the lowest energy pathway for decomposition.[46] Higher kinetic energy is required for elimination of Si from CAD of $FeSi^+$ than is required for reaction 13b. This result suggests that reaction 13b involves *direct* elimination of SiH_2 instead of sequential H_2/Si losses. For comparison, CAD of $CoSiH_2^+$ in a sector instrument (8 keV kinetic energy) yielded H (3.5%), H_2 (14.5%), and SiH_2 (82.0%) losses.[30] It was suggested that the predominant loss of SiH_2 from CAD of $CoSiH_2^+$ supports a cobalt–silylene structure. We cannot deduce the structure of $FeSiH_2^+$ from our CAD results because rearrangement often precedes fragmentation under FTMS-CAD conditions.

The reactivity of $FeSiH_2^+$ with ethene, benzene, 1,4-cyclohexadiene, and water was studied to gain structural insight. Ethene reacts with $FeSiH_2^+$ to yield dehydrogenation and adduct formation, reaction 14 ($k = (4.4 \pm 1.3) \times 10^{-10}$ cm^3 molecule^{-1} s^{-1}, eff. = 0.44). Ethene-d_4 yields significant H/D exchange, reaction 15 ($k = (9.7 \pm 2.9) \times 10^{-10}$ cm^3 molecule^{-1} s^{-1}, eff. = 0.97). These results indicate that H/D exchange (reactions 15a,b) is competitive with dehydrogenation.

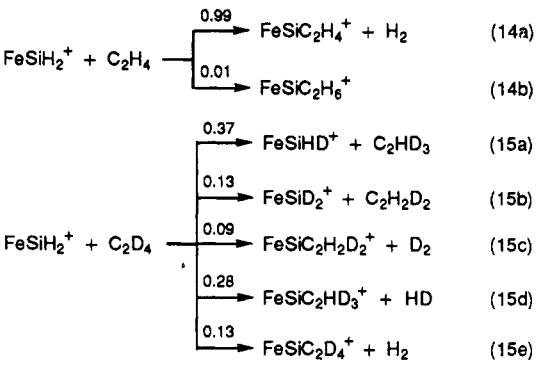

Benzene reacts with $FeSiH_2^+$ to yield exclusive dehydrogenation, reaction 16. CAD of the product of reaction 16 yields

$$FeSiH_2^+ + C_6H_6 \rightarrow FeSiC_6H_6^+ + H_2 \qquad (16)$$

exclusive elimination of C_6H_6 which indicates that $D^\circ(Fe^+–Si) > D^\circ(Fe^+–benzene) = 55 + 5$ kcal/mol.[55] 1,4-Cyclohexadiene reacts with $FeSiH_2^+$ to yield predominant SiH_4 elimination, reaction 17. Predominant silane elimination, reaction 17a, supports an

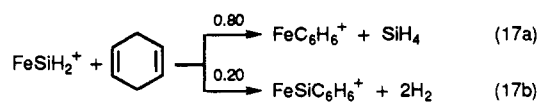

iron–silylene structure (**6a**) for $FeSiH_2^+$. Structures **6b** and **6c**

(55) Hettich, R. L.; Jackson, T. C.; Stanko, E. M.; Freiser, B. S. *J. Am. Chem. Soc.* **1986**, *108*, 5086.

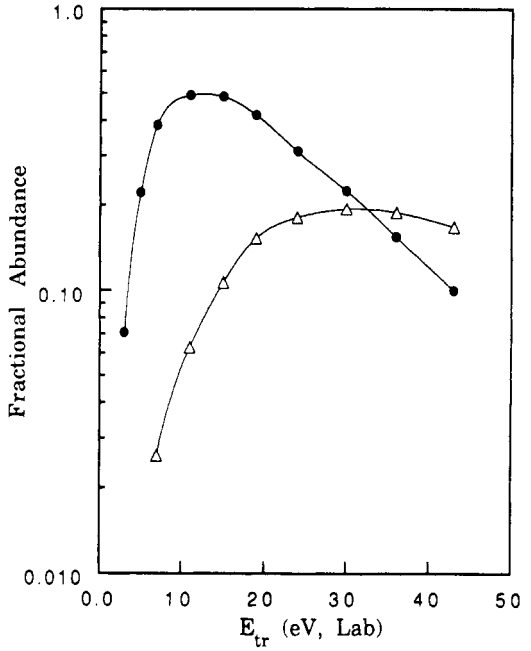

Figure 2. Plot of the variation of fragment ion abundances as a function of kinetic energy (laboratory frame) for CAD of $FeSiCH_4^+$ (**3a**) formed in reaction 4: $FeSi^+$ (●), Fe^+ (Δ).

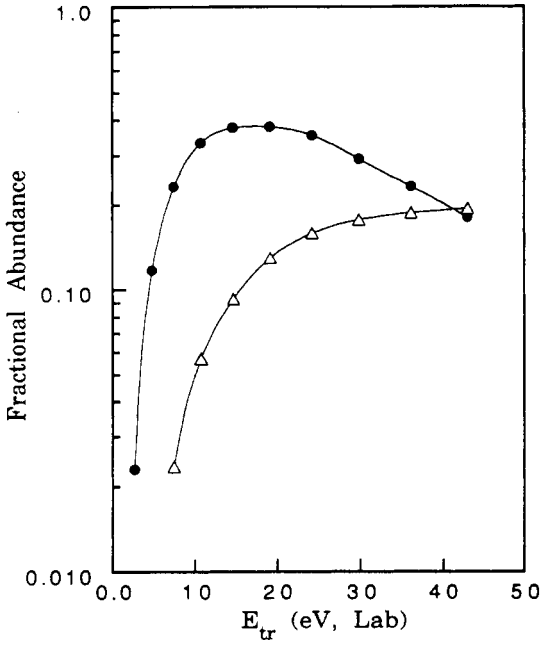

Figure 3. Plot of the variation of fragment ion abundances as a function of kinetic energy (laboratory frame) for CAD of $FeSiCH_4^+$ (**3b**) formed in reaction 7: $FeSi^+$ (●), Fe^+ (Δ).

would have been expected to yield predominant dehydrogenations, reaction 17b. Finally, H_2O reacts with $FeSiH_2^+$ by reaction 18 ($k = (2.6 \pm 0.8) \times 10^{-10}$ cm^3 molecule^{-1} s^{-1}; eff. = 0.14).

$$FeSiH_2^+ + H_2O \xrightarrow{0.38} FeOH^+ + SiH_3 \quad (18a)$$

$$\xrightarrow{0.49} FeO^+ + SiH_4 \quad (18b)$$

$$\xrightarrow{0.13} Fe^+ + (SiH_4O) \quad (18c)$$

$FeSiCH_4^+$. The CAD breakdown curves for $FeSiCH_4^+$ ions formed in reactions 4 (**3a**) and 7 (**3b**) are illustrated in Figures 2 and 3 , respectively. Both ions yield identical fragmentations, reaction 19, with similar energy dependencies and efficiencies.

$$FeSiCH_4^+ \xrightarrow{CAD} FeSi^+ + CH_4 \quad (19a)$$

$$\xrightarrow{CAD} Fe^+ + (SiCH_4) \quad (19b)$$

SORI-CAD[45] of both $FeSiCH_4^+$ions, **3a** and **3b**, yield exclusive elimination of CH_4 indicating that process 19a is the lowest energy pathway for decomposition. The CAD results suggest that either a common $FeSiCH_4^+$ structure is formed by reactions 4 and 7 or rearrangement to a common intermediate precedes fragmentation.

Although CAD does not structurally distinguish the $FeSiCH_4^+$ ions, reaction with ethene clearly establishes distinct isomeric structures for **3a** and **3b**. The results for reaction of **3a** and **3b** with ethene are summarized in Table IV. Both **3a** and **3b** yield *exclusive* adduct formation with ethene, reactions 20 and 21.

$$\mathbf{3a} + C_2H_4 \rightarrow \mathbf{3a}(C_2H_4) \quad (20)$$

$$\mathbf{3b} + C_2H_4 \rightarrow \mathbf{3b}(C_2H_4) \quad (21)$$

The rate constant for reaction 20 is significantly greater (ca. a factor of 8) than that for reaction 21 (Table IV). Adduct **3a**(C_2H_4) adds a second ethene, reaction 22 ($k = (1.0 \pm 0.5) \times$

$$\mathbf{3a}(C_2H_4) + C_2H_4 \rightarrow \mathbf{3a}(C_2H_4)_2 \quad (22)$$

10^{-10} cm^3 molecule^{-1} s^{-1}; eff. = 0.099), while adduct **3b**(C_2H_4) is inert with ethene ($k < 10^{-14}$ cm^3 molecule^{-1} s^{-1}). These dramatic differences in reactivity clearly indicate distinct structures for **3a** and **3b**; however, structural assignment would certainly be equivocal from the above information.

The structures of **3a** and **3b** were further probed by isotopic exchange reactions with ethene-d_4 and ethene-$^{13}C_2$. **3a** reacts rapidly ($k = (4.3 \pm 1.3) \times 10^{-10}$ cm^3 molecule^{-1} s^{-1}; eff. = 0.44) with ethene-d_4 to yield a predominant, *single* H/D exchange along with a small amount of multiple H/D exchange and adduct formation, reaction 23. The mass spectra for reaction of **3a** with

$$\mathbf{3a} + C_2D_4 \xrightarrow{0.12} \mathbf{3a}(C_2D_4) \quad (23a)$$

$$\xrightarrow{0.85} FeSiCH_3D^+ + C_2D_3H \quad (23b)$$

$$\xrightarrow{0.03} FeSiCH_{3-x}D_{1+x}^+ + C_2D_{3-x}H_{1+x} \quad (23c)$$

$X = 1\text{–}3$

ethene-d_4 is illustrated in Figure 4. The product of reaction 23b yields predominant adduct formation with C_2D_4 along with some additional H/D exchange, reaction 24 ($k = (1.3 \pm 0.4) \times 10^{-10}$ cm^3 molecule^{-1} s^{-1}; eff. = 0.13). A statistical distribution for H/D exchange would yield an 18.5:18.5:3.0 ratio for reactions 24b–d, respectively. This statistical distribution is in excellent

$$FeSiCH_3D^+ + C_2D_4 \xrightarrow{0.60} FeSiCH_3D(C_2D_4)^+ \quad (24a)$$

$$\xrightarrow{0.19} FeSiCH_2D_2^+ + C_2HD_3 \quad (24b)$$

$$\xrightarrow{0.17} FeSiCHD_3^+ + C_2H_2D_2 \quad (24c)$$

$$\xrightarrow{0.04} FeSiCD_4^+ + C_2H_3D \quad (24d)$$

agreement with the actual isotopic distribution. These results indicate that **3a** contains *one unique* hydrogen atom with three other, apparently equivalent, hydrogen atoms. CAD of adduct **3a**(C_2D_4) yields ethene elimination predominately as C_2HD_3 with some C_2D_4, $C_2H_2D_2$, and C_2H_3D losses also observed, consistent with reaction 23. Finally, adduct **3a**(C_2D_4) reacts with ethene-d_4 to yield exclusive addition of ethene (no H/D exchange observed).

Table IV. Summary of Kinetic Data for the Reaction of **3a**, **3b**, **4a**, **4b**, and **5** with Ethenes

reactant ion	neutral reactant	k^a	eff[b]
$FeSiCH_4$ (**3a**)	C_2H_4	0.62 (0.19)	0.06
	$^{13}C_2H_4$	1.2 (0.4)	0.12
	C_2D_4	4.3 (1.3)	0.44
$FeSiCH_4^+$ (**3b**)	C_2H_4	0.08 (0.02)	0.008
	$^{13}C_2H_4$	0.14 (0.04)	0.01
	C_2D_4	0.11 (0.03)	0.01
$FeSiC_2H_6^+$ (**4a**)	C_2H_4	0.13 (0.04)	0.01
	$^{13}C_2H_4$	0.19 (0.06)	0.02
	C_2D_4	0.29 (0.09)	0.03
$FeSiC_2H_6^+$ (**4b**)	C_2H_4	0.15 (0.04)	0.01
	$^{13}C_2H_4$	0.29 (0.09)	0.03
	C_2D_4	0.18 (0.05)	0.02
$FeSiC_3H_8^+$ (**5**)	C_2H_4	0.57 (0.17)	0.06
	$^{13}C_2H_4$	0.93 (0.28)	0.09
	C_2D_4	0.67 (0.20)	0.07

[a] Observed bimolecular rate coefficient for disappearance of reactant ion in the units of 10^{-10} cm^3 molecule^{-1} s^{-1} with uncertainty of ±30% (in parentheses). [b] Overall reaction efficiency = k_{obs}/k_{coll}. Collision rates calculated by using the average dipole orientation approximation taken from ref 77.

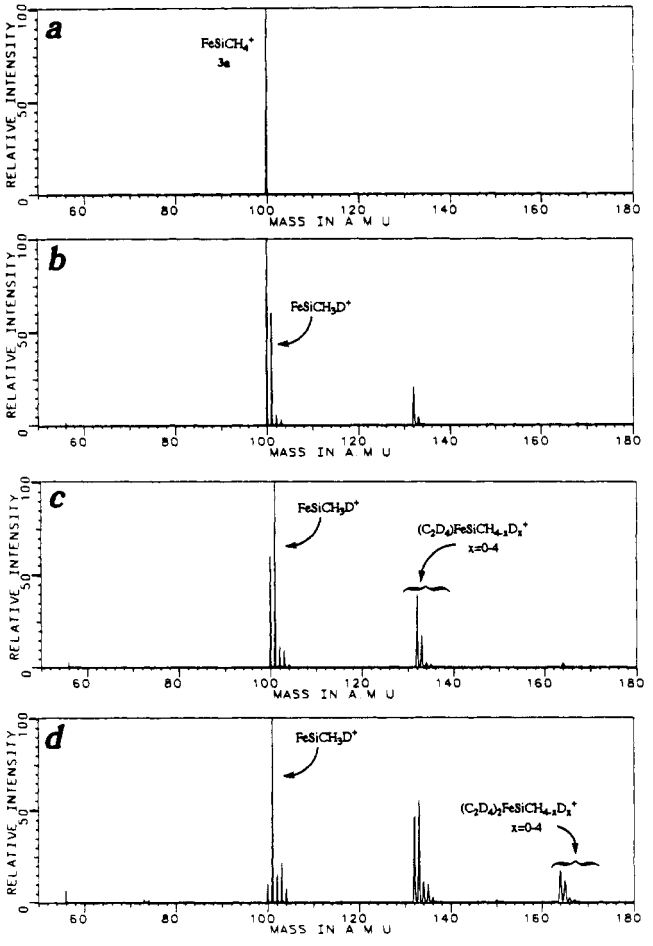

Figure 4. Spectra showing the reaction of $FeSiCH_4^+$ (**3a**) with 5.1 X 10^{-8} Torr of C_2D_4: (a) isolation of $FeSiCH_4^+$, m/z 100; (b) same as part a except a 1.0-s reaction with C_2D_4 follows isolation; (c) 2.0 s reaction with C_2D_4; (d) 5.0-s reaction with C_2D_4.

Ethene-$^{13}C_2$ reacts with **3a** to yield both adduct formation and $^{12}C/^{13}C$ exchange, reaction 25. CAD of adduct **3a**($^{13}C_2H_4$) yields

$$\mathbf{3a} + {}^{13}C_2H_4 \xrightarrow{0.42} \mathbf{3a}({}^{13}C_2H_4) \quad (25a)$$

$$\mathbf{3a} + {}^{13}C_2H_4 \xrightarrow{0.58} FeSi{}^{13}CH_4^+ + C{}^{13}CH_4 \quad (25b)$$

significant $C^{13}CH_4$ and $^{13}C_2H_4$ eliminations. Again, adduct

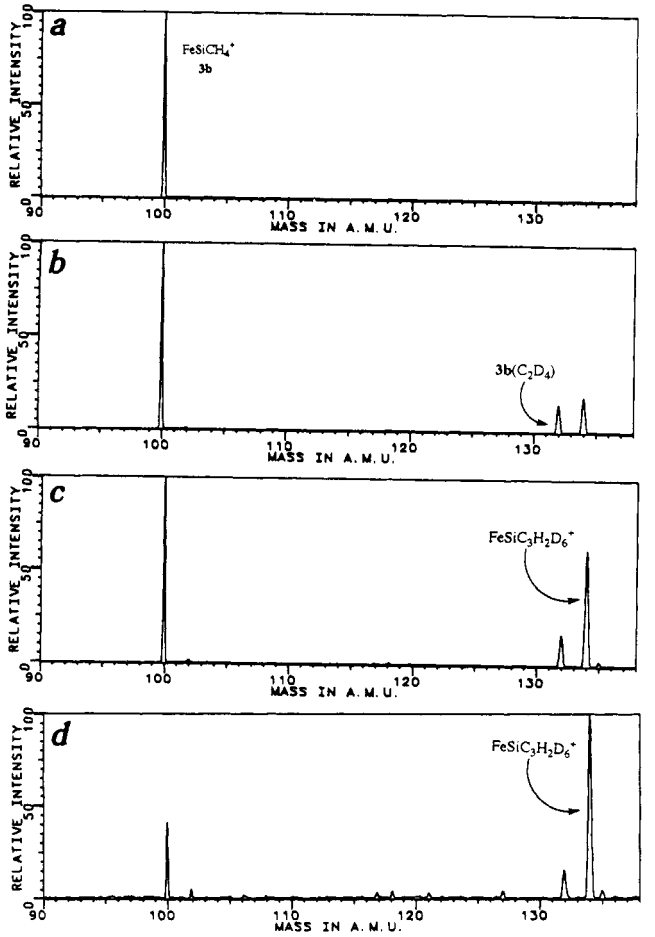

Figure 5. Spectra showing the reaction of $FeSiCH_4^+$ (**3b**) with 1.2 X 10^{-6} Torr of C_2D_4: (a) isolation of $FeSiCH_4^+$, m/z = 100; (b) same as part a except a 1.0-s reaction with C_2D_4 follows isolation; (c) 2.0-s reaction with C_2D_4; (d) 5.0-s reaction with C_2D_4.

3a($^{13}C_2H_4$) undergoes exclusive addition of a second ethene-$^{13}C_2$ (no isotopic exchange observed).

The above results suggest that **3a**, formed in reaction 4, has an iron–silylene structure (**Ia**) and *not* an iron–silene structure (**Ib**). These results suggest that β-hydrogen migration to yield structure **Ib** does not occur, Scheme I.

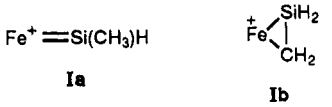

Ia **Ib**

3b reacts with ethene-d_4 to yield exclusive adduct formation, reaction 26 (k = (1.1 ± 0.3) × 10^{-11} cm^3 molecule^{-1} s^{-1}, eff. =

$$\mathbf{3b} + C_2D_4 \rightarrow \mathbf{3b}(C_2D_4) \quad (26)$$

0.011). Adduct **3b**(C_2D_4) undergoes an exclusive *double* H/D exchange with ethene-d_4 (i.e., sequential H/D exchange is *not* observed), reaction 27. The mass spectra observed for reaction

$$\mathbf{3b}(C_2D_4) + C_2D_4 \rightarrow FeSiC_3H_2D_6^+ + C_2H_2D_2 \quad (27)$$

of **3b** with ethene-d_4 are shown is Figure 5 and clearly illustrate the double H/D exchange for the adduct **3b** (C_2D_4). **3b** reacts with ethene-$^{13}C_2$ to yield exclusive adduct formation followed by $^{12}C/^{13}C$ exchange, reaction 28. The ethene-d_4 adduct of

$$\mathbf{3b}({}^{13}C_2H_4) + {}^{13}C_2H_4 \rightarrow FeSi{}^{13}C_3H_8^+ + C{}^{13}CH_4 \quad (28)$$

$FeSiCH_2D_2^+$ (**3c**) yields double H/D exchange with ethene-d_4,

Scheme VII

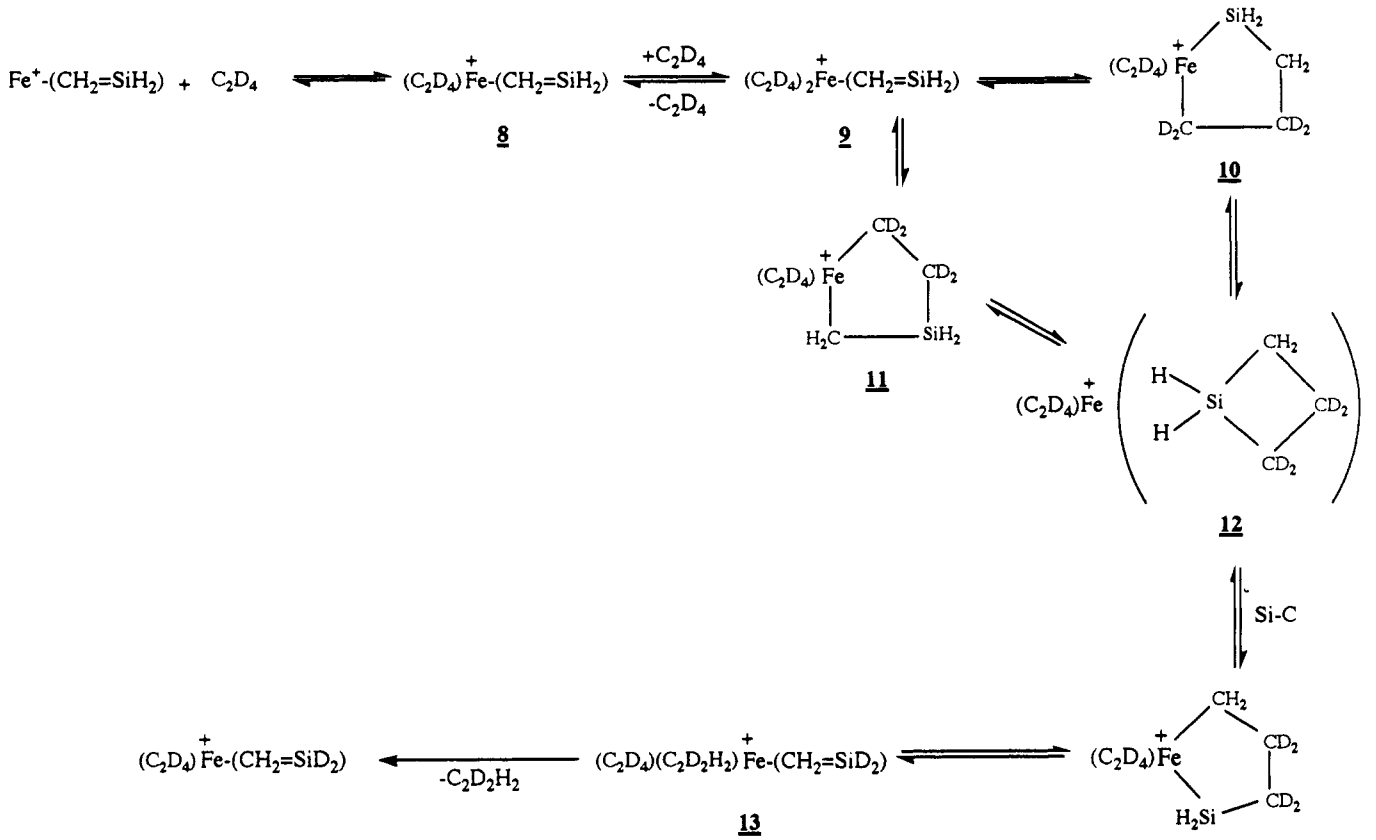

whereas **3c** (C_2H_4) does not yield H/D exchange with C_2H_4. These results are consistent with formation of an iron–silene complex (**Ib**) in reaction 7 as predicted by Scheme IV. The isotopic exchange with ethene-d_4 would involve methylene exchange between the silene and ethene.

The above isotopic exchange results are also consistent with formation of an iron–methylene–silylene complex ($H_2Si{=}Fe{=}CH_2)^+$ (**7**) in reaction 7. **7** was eliminated as a possible structure by observing the reaction of **3b** with 1,4-cyclohexadiene. Here, 1,4-cyclohexadiene will supply two hydrogen atoms to the complex which could result in hydrogenation of an iron-bound species with subsequent reductive elimination of a stable compound. For example, **7** should yield losses of CH_4, SiH_4, and H_2 whereas **Ib** should yield elimination of the silane, $(CH_3)SiH_3$, as well as dehydrogenation. **3b** reacts with 1,4-cyclohexadiene to yield predominant loss of $(CH_3)SiH_3$ along with some multiple dehydrogenation, reaction 29. The absence of CH_4 and SiH_4

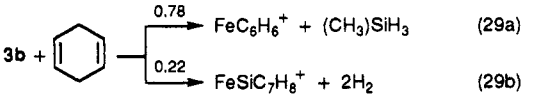

losses combined with predominant $(CH_3)SiH_3$ elimination clearly eliminates **7** as a possible structure.

We now consider the mechanism for isotopic exchange between **3b** and ethene-d_4 (ethene-$^{13}C_2$). The absence of isotopic exchange between **3b** and isotopically labeled ethene indicates that there is a prohibitive barrier for an exchange process with **3b**. However, the addition of a second ethene unit to **3b** results in isotopic exchange. A mechanism is presented in Scheme VII to account for the above isotopic exchange results. Initially, C_2D_4 forms the adduct **8**. **8** adds a second ethene-d_4 unit to form the activated species **9**. **9** may undergo C–C or C–Si bond formation to yield silametallacyclopentanes **10** and **11**, respectively. Both **10** and **11** may collapse back to **9**, however, without isotopic exchange. Isotopic exchange may proceed by reductive C–Si coupling to yield a molecular silacyclobutane–iron adduct (**12**). Subsequent oxidative addition (C–C or Si–C) of the *nascent* silacyclobutane followed by C–C bond cleavage yields **13** which contains a CD_2-CH_2 ethene group. Loss of CD_2CH_2 completes the exchange process. The mechanism in Scheme VII accounts for all the isotopic exchange results for **3b** (i.e., exclusive double H/D exchange with ethene-d_4 and $^{12}C/^{13}C$ exchange with ethene-$^{13}C_2$).

3a and **3b** yield unique reactions with both benzene and water. Benzene reacts with **3a** to yield predominant demethanation, reaction 30, whereas **3b** gives predominant dehydrogenation,

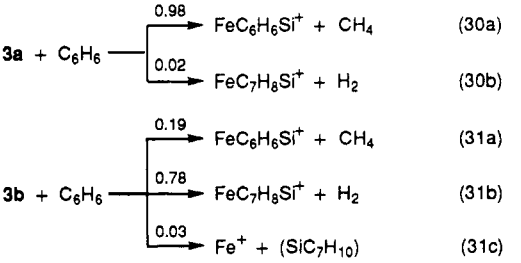

reaction 31. **3c** ($Fe(CH_2{=}SiD_2)^+$) yields dehydrogenation exclusively as D_2 loss and demethanation as CH_2D_2 loss, reaction 32. These results suggest that methane elimination is more

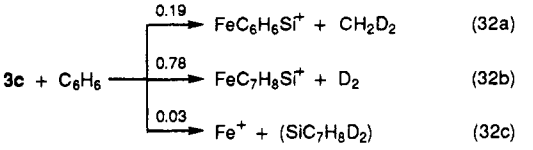

favorable for structure **Ia** and dehydrogenation is more favorable for structure **Ib**. The preference for elimination of methane from **3a** is consistent with structure **Ia** and the exclusive elimination of D_2 for dehydrogenation of **3c** is consistent with structure **Ib**.

Water reacts with **3a** and **3b** to yield both dehydrogenation and Fe^+ formation, reactions 33 and 34. Although both ions

$$\mathbf{3a} + H_2O \xrightarrow{0.27} FeSiCH_4O^+ + H_2 \quad (33a)$$
$$\mathbf{3a} + H_2O \xrightarrow{0.73} Fe^+ + (SiCH_6O) \quad (33b)$$

$$\mathbf{3b} + H_2O \xrightarrow{0.23} FeSiCH_4O^+ + H_2 \quad (34a)$$
$$\mathbf{3b} + H_2O \xrightarrow{0.77} Fe^+ + (SiCH_6O) \quad (34b)$$

yield similar branching ratios, the rate constants are quite distinct ($(1.1 \pm 0.3) \times 10^{-10}$ cm^3 molecule^{-1} s^{-1} and eff. = 0.06 for reaction 33 and $(5.8 \pm 1.7) \times 10^{-10}$ cm^3 molecule^{-1} s^{-1} and eff. = 0.32 for reaction 34). Reaction 34 may proceed by direct addition of water across the Si=C double bond to yield silanol ($(CH_3)(OH)SiH_2$). Methanol adds to $(\eta^5\text{-}C_5Me_5)(PMe_3)Ir(CH_2{=}SiPh_2)$ to yield the methoxysilyl species, $(\eta^5\text{-}C_5Me_5)(PMe_3)Ir(H)(CH_2Si(OMe)Ph_2)$.[26b] Free silenes react efficiently with water and alcohols to give addition products.[56-59]

$FeSiC_2H_6^+$. The CAD spectra for the $FeSiC_2H_6^+$ ions formed in reactions 5 (**4a**) and 8 (**4b**) are complicated with several decompositions observed, reaction 35. The CAD breakdown

$$FeSiC_2H_6^+ \xrightarrow{CAD} FeSiC_2H_4^+ + H_2 \quad (35a)$$
$$FeSiC_2H_6^+ \xrightarrow{CAD} FeSiCH_2^+ + CH_4 \quad (35b)$$
$$FeSiC_2H_6^+ \xrightarrow{CAD} FeSiH_2^+ + C_2H_4 \quad (35c)$$
$$FeSiC_2H_6^+ \xrightarrow{CAD} FeSi^+ + (C_2H_6) \quad (35d)$$
$$FeSiC_2H_6^+ \xrightarrow{CAD} Fe^+ + (SiC_2H_6) \quad (35e)$$

curves for **4a** and **4b** yield identical fragmentations, reaction 35, with similar energy dependencies and fragmentation efficiencies (Figures 6 and 7). SORI-CAD of **4a** and **4b** are similar (Figure 8) and yield losses of H_2, CH_4, and C_2H_4, reactions 35a–c. Reaction 35b is the dominant fragmentation channel at low kinetic energy for both conventional CAD and SORI-CAD. As with the $FeSiCH_4^+$ isomers, CAD fails to structurally distinguish **4a** and **4b**.

Reaction with ethene again clearly distinguishes structural isomers for **4a** and **4b**. **4a** and **4b** yield exclusive adduct formation with ethene, reactions 36 and 37 (Table IV). As with the $FeSiCH_4^+$

$$\mathbf{4a} + C_2H_4 \rightarrow \mathbf{4a}(C_2H_4) \quad (36)$$

$$\mathbf{4b} + C_2H_4 \rightarrow \mathbf{4b}(C_2H_4) \quad (37)$$

isomers (**3a** and **3b**), adduct $\mathbf{4a}(C_2H_4)$ adds a second ethene, reaction 38 ($k = (1.2 \pm 0.4) \times 10^{-11}$ cm^3 molecule^{-1} s^{-1}; eff. =

$$\mathbf{4a}(C_2H_4) + C_2H_4 \rightarrow \mathbf{4a}(C_2H_4)_2 \quad (38)$$

0.012), whereas adduct $\mathbf{4b}(C_2H_4)$ is inert with ethene ($k < 10^{-14}$ cm^3 molecule^{-1} s^{-1}). Although **4a** and **4b** have essentially identical rate constants for the initial reaction with ethene (Table IV), the secondary reactions with ethene clearly indicate formation of distinct $FeSiC_2H_6^+$ structural isomers, **4a** and **4b**.

Isotopic exchange reactions of **4a** and **4b** with ethene-d_4 and ethene-$^{13}C_2$ provide insight into ion structure. **4a** reacts with

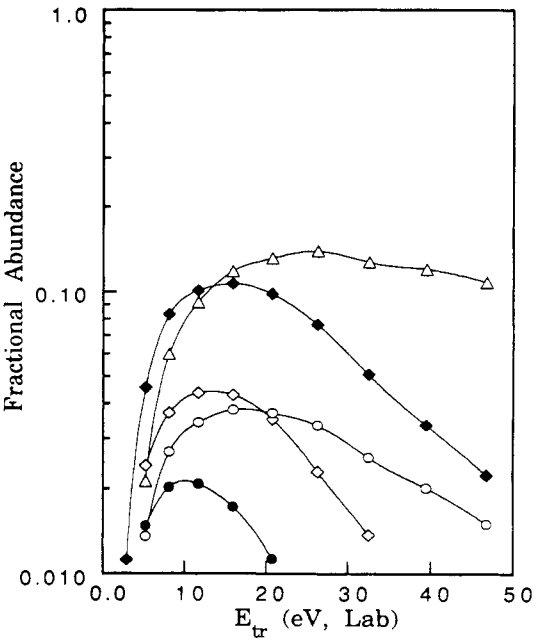

Figure 6. Plot of the variation of fragment ion abundances as a function of kinetic energy (laboratory frame) for CAD of $FeSiC_2H_6^+$ (**4a**) formed by reaction 5: $FeSiC_2H_4^+$ (●), $FeSiCH_2^+$ (◆), $FeSiH_2^+$ (◊), $FeSi^+$ (○), Fe^+ (Δ).

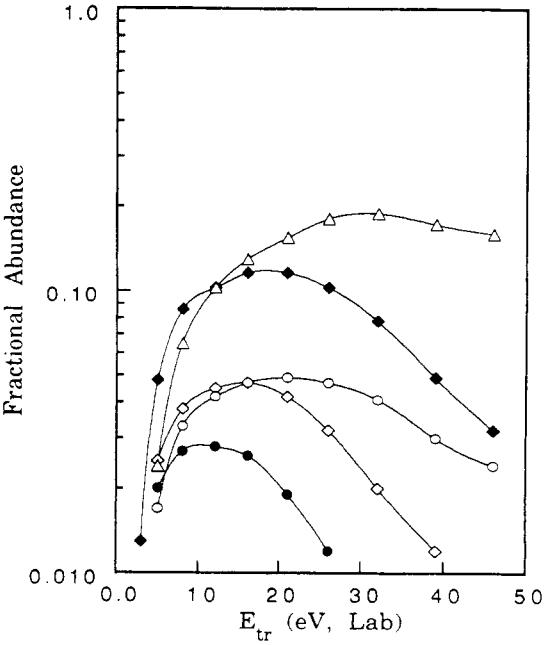

Figure 7. Plot of the variation of fragment ion abundances as a function of kinetic energy (laboratory frame) for CAD of $FeSiC_2H_6^+$ (**4b**) formed by reaction 8: $FeSiC_2H_4^+$ (●), $FeSiCH_2^+$ (◆), $FeSiH_2^+$ (◊), $FeSi^+$ (○), Fe^+ (Δ).

ethene to yield predominant adduct formation as well as H/D exchange, reaction 39 ($k = (2.9 \pm 0.9) \times 10^{-11}$ cm^3 molecule^{-1} s^{-1}). The adduct **4a** (C_2D_4) undergoes *exclusive* addition of a second ethene-d_4 unit (*no* H/D exchange observed). CAD

$$\mathbf{4a} + C_2D_4 \xrightarrow{0.64} \mathbf{4a}(C_2D_4) \quad (39a)$$
$$\mathbf{4a} + C_2D_4 \xrightarrow{0.12} FeSiC_2H_5D^+ + C_2D_3H \quad (39b)$$
$$\mathbf{4a} + C_2D_4 \xrightarrow{0.12} FeSiC_2H_4D_2^+ + C_2D_2H_2 \quad (39c)$$
$$\mathbf{4a} + C_2D_4 \xrightarrow{0.12} FeSiC_2H_3D_3^+ + C_2DH_3 \quad (39d)$$

(56) Kiro, M.; Togotaro, M.; Sakurai, H. *J. Am. Chem. Soc.* **1991**, *113*, 3986.
(57) (a) Brook, A. G.; Baines, K. M. *Adv. Organomet. Chem.* **1986**, *25*, 1. (b) Raabe, G.; Michl, J. *Chem. Rev.* **1985**, *85*, 419. (c) Guselnikov, L. E.; Nametkin, N. S. *Chem. Rev.* **1979**, *79*, 529.
(58) Brook, A. G.; Sofa, K. D.; Lickiss, P. P.; Baines, K. M. *J. Am. Chem. Soc.* **1985**, *107*, 4339.
(59) Jones, P. R.; Bates, T. F. *J. Am. Chem. Soc.* **1987**, *109*, 913.

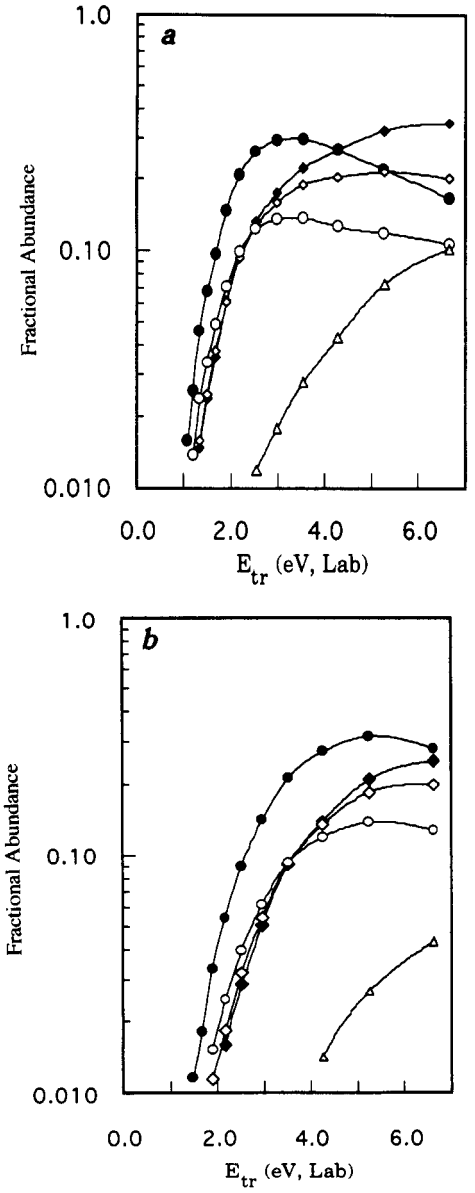

Figure 8. Plot of the variation of fragment ion abundances as a function of kinetic energy for SORI-CAD of $FeSiC_2H_6^+$ ions. CAD involves application of a 500-ms, 1.02-V electric field pulse with the maximum kinetic energy calculated directly from eq 3. The kinetic energy was varied by adjusting the frequency of the "off-resonance" pulse for (a) $FeSiC_2H_6^+$ (**4a**) formed by reaction 5 and (b) $FeSiC_2H_6^+$ (**4b**) formed by reaction 8: $FeSiC_2H_4^+$ (●), $FeSiCH_2^+$ (◆), $FeSiH_2^+$ (◊), $FeSi^+$ (○), Fe^+ (Δ).

of the adduct **4a**(C_2D_4) yields elimination of isotopically scrambled ethene, Figure 9. Ethene-$^{13}C_2$ reacts with **4a** to yield both adduct formation and $^{12}C/^{13}C$ exchange, reaction 40. The product of

$$\mathbf{4a} + {}^{13}C_2H_4 \xrightarrow{0.44} \mathbf{4a}({}^{13}C_2H_4) \quad (40a)$$

$$\mathbf{4a} + {}^{13}C_2H_4 \xrightarrow{0.56} FeSiC^{13}CH_4^+ + C^{13}CH_4 \quad (40b)$$

reaction 40b undergoes an additional $^{12}C/^{13}C$ exchange along with adduct formation. This subsequent $^{12}C/^{13}C$ exchange is not as significant as that for reaction 40 due to statistical factors. This indicates that the two carbon atoms in **4a** are equivalent. These results combined with the specific elimination of D_2 with $(CH_3)_2SiD_2$ (Table II) and the results for reaction of ethene with

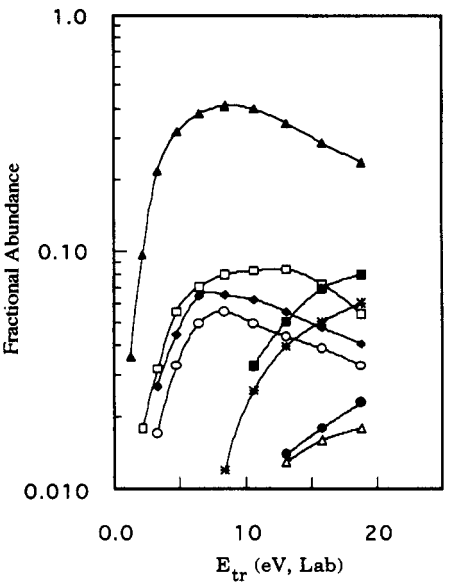

Figure 9. Plot of the variation of fragment ion abundances as a function of kinetic energy (laboratory frame) for CAD of **4a** (C_2D_4) formed by reaction 39a: $FeSiC_2H_6^+$ (▲), $FeSiC_2H_5D^+$ (◆), $FeSiC_2H_4D_2^+$ (□), $FeSiC_2H_3D_{3+}$ (○), $FeSiCH_2^+$ (*), $FeSiH_2^+$ (●), $FeSi^+$ (Δ), Fe^+ (■).

3a support an iron–silylene structure, **IIa**, for **4a**.

$$Fe^+{=}Si(CH_3)_2$$

IIa

Ethene-d_4 reacts with **4b** to yield initial, exclusive adduct formation, reaction 41 ($k = (1.8 \pm 0.5) \times 10^{-11}$ cm^3 molecule^{-1} s^{-1}). This adduct reacts with ethene-d_4 to yield exclusive *double* H/D exchange, reaction 42 (Figure 10). This double H/D

$$\mathbf{4b}(C_2D_4) + C_2D_4 \rightarrow FeSiC_4H_4D_6^+ + C_2H_2D_2 \quad (42)$$

exchange is analogous to that observed for adduct **3b**(C_2D_4) (reaction 27, Figure 5). **4b** reacts with ethene-$^{13}C_2$ to yield exclusive, initial adduct formation followed by a *single* $^{12}C/^{13}C$ exchange, reaction 43. These isotopic exchanges, reactions 42 and 43, presumably proceed by a mechanism similar to that

$$\mathbf{4b}({}^{13}C_2H_4) + {}^{13}C_2H_4 \rightarrow FeSiC^{13}C_3H_{10}^+ + C^{13}CH_4 \quad (43)$$

presented in Scheme VII. These isotopic exchange results are consistent with formation of an iron–silene complex (**IIb**) in

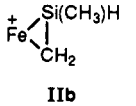

IIb

reaction 8 as predicted by Scheme IV. An iron–alkylidene–silylene $(CH_2{=}Fe{=}Si(CH_3)H)^+$ structure was eliminated from consideration by reaction with 1,4-cyclohexadiene, reaction 44.

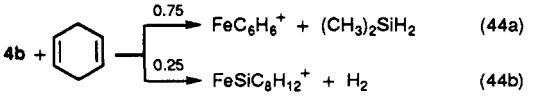

The absence of CH_4 and $(CH_3)SiH_3$ losses, combined with the predominant loss of $(CH_3)_2SiH_2$, indicates that **4b** contains a *single* moiety bound to Fe^+. For comparison, **4a** reacts similarly

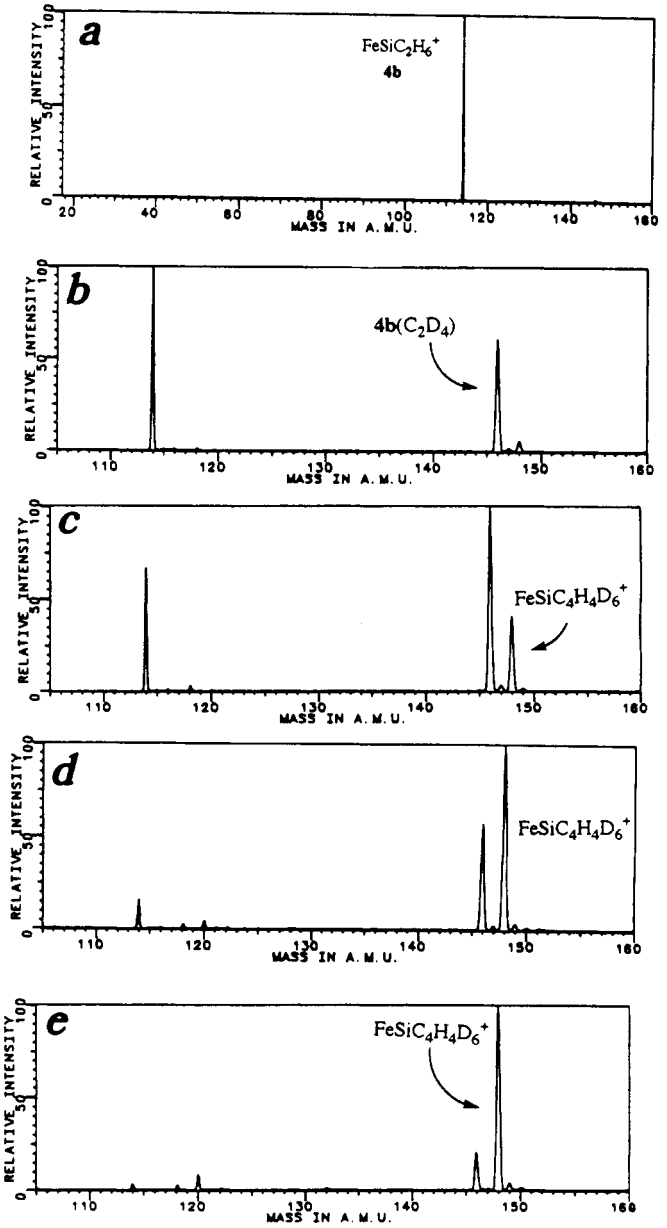

Figure 10. Spectra showing the reaction of $FeSiC_2H_6^+$ (**4b** formed by reaction 8) with 1.2×10^{-6} Torr of C_2D_4: (a) isolation of $FeSiC_2H_6^+$, m/z 114 (mass range extended to clearly show ion isolation), (b) same as part a except a 0.5-s reaction with C_2D_4 follows isolation, (c) 1.0-s reaction with C_2D_4, (d) 2.0-s reaction with C_2D_4, (e) 3.0-s reaction with C_2D_4.

with 1,4-cyclohexadiene, reaction 45. Finally, $FeSiC_2H_6^+$,

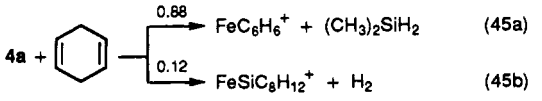

produced from $(CH_3)_6Si_2$ (reaction 11a) and $(CH_3)_3SiH$ (reaction 6b), yield identical results to those for **4a**, indicating that it consists of an iron–silylene structure (**IIa**) as predicted by the mechanisms in Schemes III and V.

In contrast to the $FeSiCH_4^+$ isomers (**3a** and **3b**), the $FeSiC_2H_6^+$ isomers (**4a** and **4b**) react similarly with benzene to yield *exclusive* adduct formation. Reaction of water with **4a** and **4b** is more complicated than that for **3a** and **3b** with several products observed, reactions 46 and 47. Both isomers yield nearly identical product distributions, however, the rate constants are quite different ($(5.6 \pm 1.7) \times 10^{-11}$ cm^3 molecule^{-1} s^{-1} and eff. = 0.03 for reaction 46

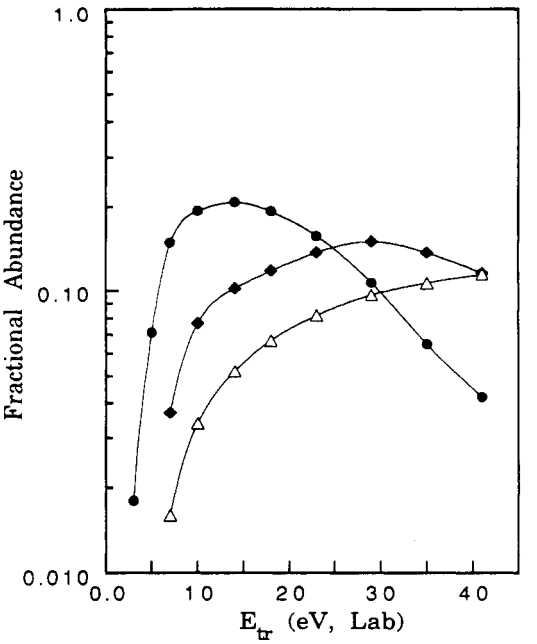

Figure 11. Plot of the variation of fragment ion abundances as a function of kinetic energy (laboratory frame) for CAD of $FeSiC_3H_8^+$ formed by reaction 9: (a) $FeSiCH_4^+$ (●), $FeSi^+$ (◆), Fe^+ (Δ).

and $(5.8 \pm 1.7) \times 10^{-10}$ cm^3 molecule^{-1} s^{-1} and eff. = 0.32 for reaction 47). This dramatic difference in rate constants is similar

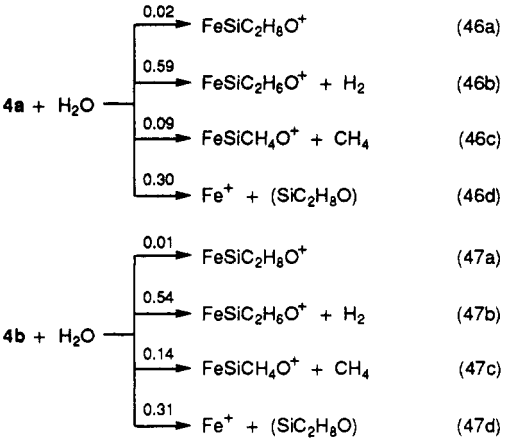

to that seen for the $FeSiCH_4^+$ isomers with the iron–silene isomer reacting more rapidly than the iron–silylene isomer.

$FeSiC_3H_8^+$. Only one $FeSiC_3H_8^+$ isomer was generated and studied (**5**, reaction 9). CAD of **5** (Figure 11) yields efficient elimination of C_2H_4, reaction 48. SORI-CAD yields exclusive elimination of C_2H_4, reaction 48, indicating that this pathway is

$$\underset{\mathbf{5}}{FeSiC_3H_8^+} \xrightarrow{CAD} FeSiCH_4^+ + C_2H_4 \qquad (48)$$

the lowest energy decomposition route. Ethene, ethene-d_4, and ethene-$^{13}C_2$ react with **5** to give exclusive adduct formation (Table IV). Adduct **5**(C_2D_4) yields a slow double H/D exchange with ethene-d_4 and adduct **5**$(^{13}C_2H_4)$ gives a *single*, slow $^{12}C/^{13}C$ exchange. These isotopic exchange reactions support an iron–silene structure (**III**) for **5**. The isotopic exchange for the ethene

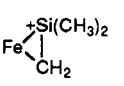

III

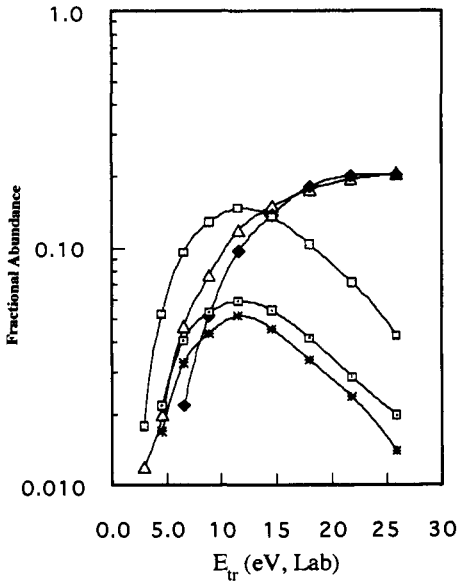

Figure 12. Plot of the variation of fragment ion abundances as a function of kinetic energy (laboratory frame) for CAD of $FeSiC_3D_6H_2^+$ formed by reaction 50: $FeSiCD_2H_2^+$ (⊡), $FeSiCD_3H^+$ (□), $FeSiCD_4^+$ (*), $FeSi^+$ (◆), Fe^+ (Δ).

adduct of **5** is significantly slower than that for the corresponding ethene adducts of **3b** and **4b**. This decreased rate of isotopic exchange may be due to steric constraints of the bound silene. $FeSiC_3H_8^+$, formed by reactions 6a and 11b, gives identical results to that of **5**, therefore, it is assigned as an iron–silene structure (**III**).

As with **4a** and **4b**, **5** reacts with benzene to yield exclusive adduct formation. Water reacts with **5** to yield predominant loss of CH_4, reaction 49 ($k = (5.3 \pm 1.6) \times 10^{-10}$ cm^3 molecule^{-1} s^{-1},

$$\mathbf{5} + H_2O \xrightarrow{0.98} FeSiC_2H_6O^+ + CH_4 \quad (49a)$$

$$\mathbf{5} + H_2O \xrightarrow{0.02} Fe^+ + (SiC_3H_{10}O) \quad (49b)$$

eff. = 0.30). This rate constant agrees quite well with that for reaction with the iron–silene species, **3b** and **4b**, *vide supra*. The isotopic exchange results combined with reaction 49 strongly support formation of an iron–silene complex (**III**) in reaction 9.

Structural studies on the product of reaction 48, $FeSiCH_4^+$, are in accord with an iron–silylene complex, **Ia**. The CAD breakdown curve for $FeSiC_3D_6H_2^+$, formed in reaction 50, is

$$Fe^+ + \langle\!\rangle\!\!-Si(CD_3)_2 \longrightarrow FeSiC_3D_6H_2^+ + C_2H_4 \quad (50)$$

illustrated in Figure 12. All three possible ethene isotopologs (C_2D_4, C_2D_3H, $C_2D_2H_2$) are eliminated in significant amounts. At a kinetic energy of 6.5 eV the distribution of ethene isotopolog eliminations, reaction 51, is nearly identical to that for a random

$$FeSiC_3D_6H_2^+ \xrightarrow{CAD} \begin{cases} \xrightarrow{0.19\ (0.214)} FeSiCD_4^+ + C_2H_2D_2 & (51a) \\ \xrightarrow{0.57\ (0.572)} FeSiCHD_3^+ + C_2HD_3 & (51b) \\ \xrightarrow{0.24\ (0.214)} FeSiCH_2D_2^+ + C_2D_4 & (51c) \end{cases}$$

isotope distribution (random distribution in parentheses). This near random isotopic distribution suggests that the hydrogen atoms in **5** are equilibrated prior to ethene elimination.

Bond Dissociation Energy. All of the reactions summarized in Table II that yield neutral losses are exothermic. Lower limits for Fe^+–(silylene/silene) bond dissociation energies can be deduced by using the thermochemical values listed in Table V combined with the structural studies. For example, reaction 52

$$Si_2H_6 \rightarrow SiH_2(^1A_1) + SiH_4 \quad (52)$$

is 55 kcal/mol endothermic, therefore, $D^\circ(Fe^+–SiH_2)$ must exceed this value, because reaction 12 is exothermic. The energy requirements for related reactions are summarized in Table VI. Displacement reactions with benzene yield additional limits on bond dissociation energies. Benzene reacts with **4a**, **4b**, and **5** to yield *exclusive* adduct formation, *vide supra*. SORI-CAD of these adducts yields exclusive loss of benzene. This indicates that $D^\circ(Fe^+–Si(CH_3)_2)$, $D^\circ(Fe^+–(CH_2=Si(CH_3)H)$, and $D^\circ(Fe^+–(CH_2=Si(CH_3)_2)$ all exceed $D^\circ(Fe^+–benzene) = 55 \pm 5$ kcal/mol.[55] **3a** and **3b** both react with benzene by elimination of neutrals (reactions 30 and 31) hence thermochemical information cannot be deduced. However, it seems reasonable that $D^\circ(Fe^+–Si(CH_3)H)$ and $D^\circ(Fe^+–(CH_2=SiH_2))$ should have similar lower bond dissociation limits to that for the $FeSiC_2H_6^+$ isomers (>55 ± 5 kcal/mol). Consequently, we assign a lower limit of 55 ± 5 kcal/mol for both $D^\circ(Fe^+–Si(CH_3)H)$ and $D^\circ(Fe^+–(CH_2=SiH_2))$.

Table V. Summary of Thermochemical Values Used in the Text

organosilane	selected ΔH_f°(298 K)[a,b]	other values[c]
SiH_4	8.2 ± 0.5[d]	
$(CH_3)SiH_3$	−7.0 ± 1.0[d]	
$(CH_3)_2SiH_2$	−23.0 ● 1.0[d]	
$(CH_3)_3SiH$	−39.0 ± 1.0[d]	
$(CH_3)_4Si$	−55.4 ± 0.8[d]	
$(CH_3)_6Si_2$	−83 ● 3[e]	−75,[k] −74.9[h]
Si_2H_6	19.1[e]	
silacyclobutane	9.3[f]	
1-methylsilacyclobutane	−7.2[g]	
1,1-dimethylsilacyclobutane	−23.8[f]	
$(CH_2=CH)SiH_3$	20.7 ± 1.0[h]	
$CH_2=CH(CH_3)SiH_2$	5[i]	
SiH_2 ($^1A_1$)	65.5 ± 1.0[j]	65.3,[l] 64.8[h]
$(CH_3)SiH$	48.8 ± 2.3[h]	48,[k] 44,[d] 51.9,[m] 50.6[n]
$(CH_3)_2Si$	32.2 ± 2.4[h]	32–33,[o] 32,[k] 25.7[e]
$CH_2=SiH_2$	40.7 ± 2.4[h]	37.0,[d] 46.5[n]
$CH_2=Si(CH_3)H$	26.4 ± 1.8[h]	21[d]
$CH_2=Si(CH_3)_2$	12.3 ± 1.4[h]	5,[d] 8.6[p]

[a] All values in kcal/mol. [b] Values used for thermochemical calculations in the text. [c] Other thermochemical values. [d] Reference 78. [e] Reference 79. [f] Reference 80. [g] Estimated by assuming a heat of formation intermediate between silacyclobutane and 1,1-dimethylsilacyclobutane. [h] Reference 81. [i] Estimated from the heat of formation of $(CH_2=CH)SiH_3$ and assuming a methyl stabilization energy of 16 kcal/mol. [j] Reference 82. [k] Reference 84. [l] Reference 83. [m] Reference 86. [n] Reference 85. [o] Reference 87. [p] Reference 88.

Table VI. Summary of Reaction Endothermicities for Formation of Silylenes and Silenes[a,b]

	ΔH°(298 K), kcal/mol
Silylene Formation	
$Si_2H_6 \rightarrow SiH_2(^1A_1) + SiH_4$	54.6
$(CH_3)SiH_3 \rightarrow (CH_3)SiH + H_2$	55.8
$CH_2=CH(CH_3)SiH_2 \rightarrow (CH_3)SiH + C_2H_4$	56.3
$(CH_3)_2SiH_2 \rightarrow (CH_3)_2Si + H_2$	55.2
$(CH_3)_3SiH \rightarrow (CH_3)_2Si + CH_4$	53.4
$(CH_3)_6Si_2 \rightarrow (CH_3)_2Si + (CH_3)_4Si$	59.8
Silene Formation	
silacyclobutane $\rightarrow CH_2=SiH_2 + C_2H_4$	43.9
1-methylsilacyclobutane $\rightarrow CH_2=Si(CH_3)H + C_2H_4$	46.1
1,1-dimethylsilacyclobutane $\rightarrow CH_2=Si(CH_3)_2 + C_2H_4$	48.6
$(CH_3)_3SiH \rightarrow CH_2=Si(CH_3)_2 + H_2$	51.3

[a] Heats of formation for silicon containing species taken from Table V. [b] Auxiliary thermochemical information taken from ref 89.

Table VII. Summary of Branching Ratios for Reaction of Fe^+–(Silylene/Silene) with 1-Butene

reactant ion	product ions[a]	$D°(Fe^+$–(silylene/silene))[b]
Fe^+=SiH_2	$FeC_4H_6^+$ (0.46) $FeSiC_3H_6^+$ (0.12) $FeSiC_3H_4^+$ (0.11) $FeSiC_2H_6^+$ (0.01) $FeSiCH_4^+$ (0.30)	<79
Fe^+=$Si(CH_3)H$ (**3a**)	$FeC_4H_6^+$ (0.42) $FeSiC_5H_{10}^+$ (0.10) $FeSiC_4H_8^+$ (0.17) $FeSiC_3H_8^+$ (0.02) $FeSiC_2H_6^+$ (0.29)	<78
Fe^+=$Si(CH_3)_2$ (**4a**)	$FeC_4H_6^+$ (0.33) $FeSiC_6H_{12}^+$ (0.08) $FeSiC_5H_{10}^+$ (0.14) $FeSiC_3H_8^+$ (0.45)	<77
Fe^+—(CH_2=SiH_2) (**3b**)	$FeC_4H_6^+$ (0.61) $FeSiC_5H_{10}^+$ (0.08) $FeSiC_4H_8^+$ (0.13) $FeSiC_3H_8^+$ (0.02) $FeSiC_2H_6^+$ (0.16)	<70
Fe^+—(CH_2=$Si(CH_3)_2$) (**4b**)	$FeC_4H_6^+$ (0.37) $FeSiC_6H_{12}^+$ (0.08) $FeSiC_5H_{10}^+$ (0.14) $FeSiC_3H_8^+$ (0.41)	<71
Fe^+—(CH_2=$Si(CH_3)_2$) (**5**)	$FeC_4H_6^+$ (0.74) $FeSiC_7H_{14}^+$ (0.02) $FeSiC_5H_{12}^+$ (0.14) $FeSiC_4H_{10}^+$ (0.02) Fe^+ (0.08)	<73

[a] Branching ratios for reactions are in parentheses. [b] Upper limit for $D°(Fe^+$–(silylene/silene)) in kcal/mol. See text for discussion.

Table VIII. Summary of Bond Dissociation Limits for Fe^+–(Silylene/Silene) Species (in kcal/mol)

$55 < D°(Fe^+–SiH_2) < 79$
$56 < D°(Fe^+–Si(CH_3)H) < 78$
$55 < D°(Fe^+–(CH_2=SiH_2)) < 70$
$60 < D°(Fe^+–Si(CH_3)_2) < 77$
$55 < D°(Fe^+–(CH_2=Si(CH_3)H)) < 71$
$55 < D°(Fe^+–(CH_2=Si(CH_3)_2)) < 73$

Upper limits for bond dissociation energies were determined by studying reaction of the Fe(silylene/silene)$^+$ ions with 1-butene where reaction 53 allows an upper limit to the bond dissociation

$$Fe(silylene/silene)^+ + 1\text{-butene} \rightarrow FeC_4H_6^+ + silane \quad (53)$$

energy to be assigned. The Fe^+–butadiene bond dissociation energy (48 ± 5 kcal/mol)[55] combined with the heat of formation of silane and 1-butene yields a lower limit for the heat of formation of the Fe(silylene/silene)$^+$ species (assuming reaction 53 is exothermic). The reactions of 1-butene with Fe(silylene/silene)$^+$ species are summarized in Table VII along with upper limits for $D°(Fe^+$–silylene/silene).

Table VIII summarizes the bond dissociation limits for Fe(silylene/silene)$^+$ species. An upper limit of 68 kcal/mol was previously assigned for $D°(Fe^+–SiH_2)$ using a beam instrument.[30,60] This value was deduced by observing that formation of $FeSiH_2^+$ was endothermic and assuming that reaction 54 was

$$Fe^+ + (CH_3)_2SiH_2 \rightarrow FeSiH_2^+ + C_2H_6 \quad (54)$$

responsible for its formation. However, it is probable that $FeSiH_2^+$ was formed from the sequential process, reaction 55, based on the CAD results for $FeSiC_2H_6^+$ ions (reaction 35, Figures 6.13, 6.14, and 6.15). The endothermicity for reaction 55 would place

$$Fe^+ + (CH_3)_2SiH_2 \xrightarrow{-H_2} FeSiC_2H_6^+ \xrightarrow{-C_2H_4} FeSiH_2^+ \quad (55)$$

an upper limit of 101 kcal/mol for $D°(Fe^+$-$SiH_2)$. In addition to process 55, it is likely that there are barriers to reaction 54 in excess of the energy required for ethane elimination. Consequently, we believe that the upper limit for $D°(Fe^+–SiH_2)$ of 68 kcal/mol needs to be revised upward to 79 kcal/mol.

Nature of the (Fe–Silylene)$^+$ and (Fe–Silene)$^+$ Bonds. SiH_2 has a ground state singlet ($^1A_1$) with the lowest lying triplet state ca. 21 kcal/mol higher.[61-63] Methyl groups increase the singlet–triplet splitting in silylene with this difference ca. 25 kcal/mol for $(CH_3)_2Si$.[64] Based on this large energy difference it is expected that the bonding in Fe(silylene)$^+$ would be dominated by σ-donation from silylene into an empty Fe^+ 4s orbital with π-back donation from a filled iron 3d orbital into the empty p orbital of Si. This requires interaction with an Fe^+ with a $3d^7$ configuration, presumably the low lying ^4F state (Table I). Hence, the Fe(silylene)$^+$ complexes can be described as consisting of a double bond with σ-donation and π-back donation.

Theory has revealed that the nature of bonding in $MSiH_2^+$ species is much more complicated than the above simple description.[65] These calculations indicate that there are four important resonance contributors to the electronic structure of $FeSiH_2^+$. The resonance structures are denoted by using the $|ijkl\rangle$ notation where i, j, k, and l are the occupation numbers of the "AO-like" MOs σ_{Si}, π_{Si}, π_{Fe}, and σ_{Fe}, respectively. Cundari and Gordon found that the configurations $|2110\rangle$ (Fe⟝Si), $|1111\rangle$ (Fe=Si), $|2020\rangle$ (Fe⇄Si), and $|1021\rangle$ (Fe⟞Si) are all important resonance contributors.[65] The upper line (or arrow) describes the π-bond; the lower line (or arrow) describes the σ-bond. The simple discussion above only considered the $|2020\rangle$ (Fe⇄Si) configuration. The natural orbital occupation numbers (NOON) for $FeSiH_2^+$ are 1.98 (σ_{FeSi}), 1.75 (π_{FeSi}), 0.25 (π^*_{FeSi}), and 0.08 (σ^*_{FeSi}).[65] Hence, the bonding in $FeSiH_2^+$ is essentially a double bond with numerous resonance contributors. It has been found that changing substituents of the silylene has little effect on the nature of the bonding.[66] Consequently, the bonding for silylenes, **3a** and **4a**, can be described in a similar fashion to that for $FeSiH_2^+$. It is interesting that the $|2020\rangle$ configuration dominates for both $CoSiH_2^+$ and $NiSiH_2^+$ and the fully covalent configuration $|1111\rangle$ dominates for $MnSiH_2^+$.[65]

The limit on the bond dissociation energies for the Fe^+–silylene species (Table VIII) is somewhat less than that for the corresponding methylidene species ($D°(Fe^+–CH_2)$ = 83.9 kcal/mol).[67] This result is consistent with that predicted from force constants for the two species ($FeSiH_2^+$ and $FeCH_2^+$).[65]

The nature of the bonding between transition metal complexes and silenes has not been investigated by theory. η^2-Silene complexes may be characterized as either metallacyclopropane (**1**) or π-silene complexes (**2**),[68] depending on the extent of back donation of electron density. Lewis and Wrighton supported a metallacyclopropane structure for $(\eta^5$-$C_5R_5)(CO)_2W(H)(CH_2$=$SiMe_2)$ based on ^1H and ^{13}C NMR chemical shifts.[25a] The π-bond energy for C=Si species (35.6 kcal/mol) is significantly less than

(60) An upper limit of 72 kcal/mol was originally assigned for $D°(Fe^+$-$SiH_2)$ (ref 30). An upper limit of 68 kcal/mol is obtained by using the thermochemical values in Table V.

(61) Berkowitz, J.; Greene, J. P.; Cho, H.; Ruscia, B. *J. Chem. Phys.* **1987**, *86*, 1235.
(62) (a) Balasubramanian, K.; McLean, A. D. *J. Chem. Phys.* **1986**, *85*, 5117. (b) Allen, W. D.; Schaefer, H. F. *Chem. Phys.* **1986**, *108*, 243.
(63) (a) Bauschlicher, C. W., Jr.; Taylor, P. R. *J. Chem. Phys.* **1986**, *85*, 6510. (b) Bauschlicher, C. W., Jr.; Taylor, P. R. *J. Chem. Phys.* **1987**, *86*, 1420. (c) Bauschlicher, C. W., Jr.; Laughoff, S. R.; Taylor, P. R. *J. Chem. Phys.* **1987**, *87*, 387.
(64) Grev, R. S.; Schaefer, H. F. *J. Am. Chem. Soc.* **1986**, *108*, 5804.
(65) Cundari, T. R.; Gordon, M. S. *J. Phys. Chem.* **1992**, *96*, 631.
(66) Cundari, T. R.; Gordon, M. S. *Organometallics* **1992**, *11*, 3122.
(67) Boo, B. H.; Armentrout, P. B. *J. Am. Chem. Soc.* **1991**, *113*, 6401.
(68) For a description of the Dewar–Chatt–Duncanson model, see: (a) Dewar, M. J. S. *Bull. Soc. Chim. Fr.* **1951**, *18*, C71. (b) Chatt, J.; Duncanson, L. A. *J. Chem. Soc.* **1953**, 2939.

that for the corresponding C=C species (65.4 kcal/mol).[69] Hence, there is a strong preference for sp^3 hybridization for silenes which should favor a metallasilacyclopropane structure. The lower limit for $D^o(Fe^+-(CH_2=SiH_2))$ of 55 kcal/mol (Table VIII) is significantly greater than the bond dissociation energy for the related ethene complex ($D^o(Fe^+-(CH_2=CH_2)) = 39.9 \pm 1.4$ kcal/mol).[70] The bonding for silenes to Fe^+ may be best characterized as a metallacyclopropane structure (**1**) based on the propensity for sp^3 hybridization for silenes and the strong Fe^+–silene bond energy. Alternatively, the bonding may be attributed primarily to **2** where the increase in the Fe^+–silene bond dissociation energy over the Fe^+–ethene dissociation energy is due to the difference in the π-bond energies for Si=C and C=C. In this case, both silene and ethene may have similar electron donor abilities; however, because the π-bond energy in Si=C is much less than that for C=C, there will be less of a decrease in the Si–C bond energy due to donation of π-electron density to the metal. Obviously, theory will yield important insights into the nature of bonding in the silene complexes.

Decomposition of $FeSiCH_4^+$, $FeSiC_2H_6^+$, and $FeSiC_3H_8^+$. The $FeSiCH_4^+$ ions (**3a** and **3b**) have identical CAD breakdown curves (Figures 2 and 3). SORI-CAD indicates that the lowest energy fragmentation channel is methane loss, reaction 19a. A new decomposition channel (dehydrogenation) is observed for reaction of **3a** and **3b** with benzene, reactions 30b, 31b, and 32b. Whereas **3a** yields nearly exclusive methane loss with benzene (reaction 30), **3b** yields predominant dehydrogenation (reaction 31). This indicates that the mode of decomposition of $FeSiCH_4^+$ ions is dramatically affected by benzene coordination. The silicon hydrogens are clearly responsible for the dehydrogenation as indicated by reaction 32b. It is surprising that Fe^+ forms two stable isomers with $SiCH_4$, **Ia** and **Ib**, which do not readily interconvert. In principal, it should be possible to convert a less stable isomer to a more stable (thermodynamic) species by careful ion activation, provided the barrier for isomerization is less than the energy required for decomposition.[71] Recently, we demonstrated the efficient isomerization of $(C_2H_5)SiH_2^+$ to $(CH_3)_2SiH^+$ by collisional activation by using an "off-resonance" electric field pulse.[72] In this case, the two $SiC_2H_7^+$ isomers were distinguished by reaction with ethene-d_4 and methanol.[73] Here, we applied an "off-resonance" electric field pulse (500 ms duration) to collisionally activate **3a** and **3b**. Following collisional activation, the structure of the $FeSiCH_4^+$ ions was probed by reaction with ethene-d_4. There was *no* evidence for interconversion between **Ia** and **Ib**, even under collisional activation energies yielding significant ion fragmentation. This implies that there is a prohibitive barrier to ion rearrangement. This result suggests that the barrier for isomer interconversion is greater than the energy required for methane loss (i.e., all ions with sufficient energy to isomerize also decompose). High-level *ab initio* theory indicates that $SiCH_4$ isomers (silene and silylene) have similar thermodynamic stability (less than 10 kcal/mol difference) (Table V). Furthermore, there is a significant barrier (ca. 40 kcal/mol) for interconversion of these $SiCH_4$ isomers.[74,75] There is clearly a prohibitive barrier for this interconversion mediated by Fe^+, $Fe(ethene)^+$, and $Fe(benzene)^+$.

In contrast to SORI-CAD of $FeSiCH_4^+$ (**3a** and **3b**), $FeSiC_2H_6^+$ isomers (**4a** and **4b**) yield several neutral losses, reactions 35a–e (Figure 8a,b). This suggests that there is a significant barrier for initial rearrangement which allows several channels (reactions 35a–e) to compete kinetically. We employed "off-resonance" irradiation for collisional activation, in an attempt to induce isomerization between **IIa** and **IIb**. Again, there was *no* evidence for isomerization. Interestingly, benzene reacts with both **4a** and **4b** to yield *exclusive* adduct formation indicating that the binding energy of benzene to **4a** and **4b** is insufficient to induce fragmentation.

In contrast to **4a** and **4b**, **5** yields very simple fragmentations upon CAD with ethene loss (reaction 48) the lowest energy pathway for decomposition. $FeSiCH_4^+$, produced by reaction 48, consists exclusively of an Fe^+–silene complex, **Ib**. Again, benzene reacts with **5** to give exclusive adduct formation indicating that there is insufficient energy in the collision complex to induce ethene elimination.

Conclusions

The *first* examples of generation and characterization of isomeric iron–silylene and iron–silene cationic complexes ($FeSiCH_4^+$ and $FeSiC_2H_6^+$) were described. These complexes were generated *in situ*, and their structures were probed by specific ion/molecule reactions with labeled ethene. Metal–silene complexes can be formed by reaction of Fe^+ with silacyclobutanes, where ethene elimination yields the metal–silene complex. Metal–silylene complexes were formed by reaction of Fe^+ with ethenylsilanes, where ethene loss generates the silylene species, and by 1,1-dehydrogenation of $(CH_3)_2SiH_2$. Collision-activated dissociation (CAD) failed to provide structural information. The similarities (same products and energy dependency) between CAD breakdown curves of $FeSiCH_4^+$ and $FeSiC_2H_6^+$ isomers imply that rearrangement to common intermediates precedes fragmentation.

There was *no* evidence for interconversion of iron–silylene and iron–silene species, even upon slow collisional activation (using SORI-CA), or by formation of ethene collision complexes (ca. 40 kcal/mol excess of energy). This is suggestive of a prohibitive barrier for iron mediated interconversion of silene and silylene.

Bond dissociation energies of the above isomeric species were bracketed by reactions with benzene and 1-butene (Table VIII). The ability to generate stable iron–silylene and –silene cations in the gas phase allows for studies concerning their role in important chemical transformations of silicon compounds.

Acknowledgment. Acknowledgment is made to the National Science Foundation NSF-EPSCoR (Grant RII-8610750) for partial support of this research.

(69) Schmidt, M. W.; Truong, P. N.; Gordon, M. S. *J. Am. Chem. Soc.* **1987**, *109*, 5217.
(70) Armentrout, P. B.; Clemmer, D. E. In *Energetics of Organometallic Species*, Simoes, J. A. M., Ed.; Kluwer: Netherlands, 1992, p 321.
(71) Hart, K. J.; McLuckey, S. A.; Glish, G. L. *J. Am. Soc. Mass Spectrom.* **1992**, *3*, 680.
(72) Bakhtiar, R.; Holznagel, C. M.; Jacobson, D. B. *Organometallics* **1993**, *12*, 621.
(73) Holznagel, C. M.; Bakhtiar, R.; Jacobson, D. B. *J. Am. Soc. Mass Spectrom.* **1991**, *2*, 278.
(74) (a) Goddard, J. D.; Yoshioka, Y.; Schaefer, H. F., III *J. Am. Chem. Soc.* **1980**, *102*, 7644. (b) Yoshioka, Y.; Schaefer, H. F., III *J. Am. Chem. Soc.* **1981**, *103*, 7366.
(75) Kohler, H. J.; Lischka, H. *J. Am. Chem. Soc.* **1982**, *104*, 5884.
(76) Coliss, C.; Sugar, J. *J. Phys. Chem. Ref. Data* **1982**, *11*, 135.
(77) Su. T.; Bowers, M. T. In *Gas Phase Ion Chemistry*, Bowers, M. T., Ed.; Academic Press: New York, 1979; Vol. 1, Chapter 3.
(78) Walsh, R. In *The Chemistry of Organic Silicon Compounds*, Patai, S., Rapport, S., Eds.; Wiley: New York, 1989, Chapter 5.
(79) Walsh, R. *Organometallics* **1989**, *8*, 1973.
(80) Gordon, M. S.; Boatz, J. A.; Walsh, R. *J. Phys. Chem.* **1989**, *93*, 1584.
(81) Allendorf, M. D.; Melius, C. F. *J. Phys. Chem.* **1992**, *96*, 428.
(82) Moffat, H. K.; Jensen, K. F.; Carr, R. W. *J. Phys. Chem.* **1991**, *95*, 145.
(83) Frey, H. M.; Walsh, R.; Watts, I. M. *J. Chem. Soc., Chem. Commun.* **1986**, 1189.
(84) O'Neal, H. E.; Ring, M. A.; Richardson, W. H.; Licciardi, G. F. *Organometallics* **1989**, *8*, 1968.
(85) Boatz, J. A.; Gordon, M. S. *J. Phys. Chem.* **1990**, *94*, 7331.
(86) Neudorfl, P. S.; Loun, E. M.; Safarik, I.; Jodhan, A.; Strausz, O. P. *J. Am. Chem. Soc.* **1987**, *109*, 5780.
(87) Boatz, J. A.; Gordon, M. S. *Organometallics* **1989**, *8*, 1978.
(88) Brix, T.; Arthur, N. L.; Potzinger, P. *J. Phys. Chem.* **1989**, *93*, 8193.
(89) Lias, S. G.; Bartmess, J. E.; Lubman, J. F.; Holmes, J. L.; Levin, R. D.; Mallard, W. G. *J. Phys. Chem. Ref. Data* **1988**, *17*, Suppl. No. 1.